SULPHUR DIOXIDE OXIDATION IN A RAINBAND:
EFFECTS OF IN-CLOUD HYDROGEN PEROXIDE PRODUCTION

by

Anne Marie Macdonald

A thesis submitted to
the Faculty of Graduate Studies and Research
in partial fulfillment of the
requirements for the degree of

MASTER OF SCIENCE

Department of Meteorology
McGill University
Montreal, Quebec

July, 1989

Choices for short title:

1)

SO_2 OXIDATION IN A RAINBAND:
EFFECTS OF IN-CLOUD H_2O_2 PRODUCTION

2)

OXIDATION IN A RAINBAND:
EFFECTS OF IN-CLOUD PEROXIDE PRODUCTION

ABSTRACT

The role of H_2O_2 in the oxidation of SO_2 in a rainband is investigated with a two-dimensional numerical model. In-cloud production of H_2O_2 was introduced in the model and results are compared to a base simulation in which the aqueous-phase H_2O_2 came from the dissolution of gaseous H_2O_2.

In the base run, H_2O_2 initially dominated as oxidant but its contribution to sulphate formation decreased as the H_2O_2 became depleted. Estimation of gas-phase concentrations of precursor HO_2 radicals with a set of gas-phase reactions, transfers of the radicals to cloud and subsequent aqueous reaction yielded H_2O_2 production rates of about 0.1-0.3 ppbv/h with increased rates higher in the rainband. The additional H_2O_2 effected a 10% and a 23% increase in the amount of SO_4^{2-} formed in cloud and rain respectively. Only a 3% increase in SO_4^{2-} deposition was observed because of the importance of nucleation of SO_4^{2-} in both simulations.

RESUME

On examine le rôle du H_2O_2 dans l'oxydation du SO_2 dans une bande de pluie à l'aide d'un modèle numérique en deux dimensions. La production de H_2O_2 dans le nuage fut introduite dans le modèle et les résultats sont comparés à une simulation témoin où le H_2O_2 en phase aqueuse provenait de la dissolution du H_2O_2 en phase gazeuse.

Dans la simulation témoin, le H_2O_2 domine initialement comme oxydant mais sa contribution à la formation de sulfate diminue à mesure que le H_2O_2 faiblit. Á l'aide d'un ensemble de réactions en phase gazeuse, on estime les concentrations des radicaux précurseurs HO_2. Le transfert de ces radicaux au nuage et les réactions aqueuses subséquentes donnent des taux de production d'environ 0.1 à 0.3 ppbv/h (partie par milliard par heure en volume) avec des taux supérieurs dans la région plus haut dans la bande de pluie. Le H_2O_2 additionel a provoqué une augmentation de 10% et 23% du SO_4^{2-} formé dans la zone de nuages et la zone de pluie respectivement. Une augmentation de seulement 3% du taux de déposition du SO_4^{2-} fut observée à cause de la domination de la nucléation du SO_4^{2-} dans les deux simulations.

ACKNOWLEDGEMENTS

It is with pleasure that I thank my thesis advisor, Dr. Henry Leighton, whose advice, useful criticisms, and continued encouragement are sincerely appreciated.

I would like to thank Alain Robichaud for translating the abstract.

I also acknowledge NSERC for providing financial assistance in the form of a Postgraduate scholarship.

TABLE OF CONTENTS

Abstract i

Résumé ii

Acknowledgements iii

Table of Contents iv

List of Figures vi

List of Tables ix

List of Symbols x

Chapter 1. AN OVERVIEW OF CLOUD CHEMISTRY MODELS 1

1.1 Introduction 1
1.2 Cloud chemistry models 3
  1.2.1 Chemistry 3
  1.2.2 Microphysics 4
  1.2.3 Dynamics 6
1.3 Modelling aqueous-phase H_2O_2 production 7
1.4 Purpose of thesis 8

Chapter 2. DESCRIPTION OF BASE SIMULATION 10

2.1 Introduction 10
2.2 Chemistry model 12
  2.2.1 Continuity equations 12
  2.2.2 Chemical species modelled 13
  2.2.3 Solubility constants and aqueous-phase equilibria 14
  2.2.4 Oxidation reactions 16
2.3 Results of base simulation 20
  2.3.1 Dynamics 20
  2.3.2 Sulphate in cloud and rain 20
    a) Nucleation and scavenging of sulphate 20
    b) Oxidation of SO_2 22
    c) Comparison with observations 24

Chapter 3. IN-CLOUD H_2O_2 PRODUCTION 36

3.1 Introduction 36
3.2 Mass transfer 37
3.3 Gas-phase production and destruction rates of HO_2 40

3.4 Actinic fluxes and ozone photolysis rates . . . 44
3.4.1 Photolysis rate coefficients 44
3.4.2 Definition of actinic flux 44
3.4.3 Model used for δ-Eddington approximation 45
a) Ozone absorption 47
b) Rayleigh scattering 48
c) Extinction by cloud 48
3.4.4 Results 50
3.5 Aqueous-phase reactions 55

Chapter 4. RESULTS OF SIMULATION WITH H_2O_2 PRODUCTION . 59

4.1 Introduction 59
4.2 Sources of H_2O_2 to drops 60
4.3 Rates of H_2O_2 production 61
4.4 Results of H_2O_2 source on sulphate production 62

Chapter 5. SUMMARY AND CONCLUSIONS 74

5.1 Introduction 74
5.2 Overview 75
5.3 Limitations of the parameterization method 78
5.4 Suggestions for further research 79

References 80

LIST OF FIGURES

Figure 2.1 17

Comparison of rate constants as a function of pH for oxidation of S(IV) by O_3. (T = 298 K). Rate constants from (a) Maahs (1983)
(b) Martin (1983)

Figure 2.2 19

Fractional rate of oxidation of S(IV) by (a) 1 ppb H_2O_2, (b) 50 ppb O_3, vs solution pH (T = 285 K).

Figure 2.3 21

Vertical cross-section of rainwater concentration at 90 minutes simulation time. Contour interval is 0.4 g/m^3. Broken line denotes cloud boundary.

Figure 2.4 27

Cloud sulphate budget: Moles of sulphate transferred from air to cloud (T_{AC}), cloud to air (T_{CA}), cloud to rain (T_{CR}). Sulphate formed in cloud by oxidation mechanism is OX_C.

Figure 2.5 28

Rain sulphate budget: Moles of sulphate formed in rain (OX_R) during simulation and transfers of sulphate involving rain. T_{CR} - cloud to rain T_{RA} - rain to air, T_{AR} - air to rain. T'_{CR} is sulphate transferred cloud to rain during simulation with no in-cloud oxidation.

Figure 2.6 29

Total moles of sulphate formed in cloud and rain by oxidation of S(IV) by H_2O_2 (solid lines) or O_3 (dashed lines).

Figure 2.7 30

(a) Total rate of sulphate production per volume of cloud water by H_2O_2 (solid line) and O_3 (dashed line), vs time.

(b) Same as 2.7a but for rain.

Figure 2.8 31

(a) Total rate of in-cloud oxidation (moles/s) of S(IV) by H_2O_2 at cloud base (1250 m) and 1 km above cloud base (2250 m).

(b) Same as 2.8a but oxidation by O_3.

Figure 2.9 32

Average concentration of H_2O_2 (mg/L) dissolved in cloud at 1250 m and 2250 m, vs time.

Figure 2.10 32

Average pH in cloud at levels 1250 m and 2250 m, vs time.

Figure 2.11 33

(a) Total in-rain oxidation rate of S(IV) by H_2O_2 (moles/s) at 2250 m, 1250 m, and 1 km below cloud base at 250 m.

(b) Same as 2.11a but oxidation by O_3 at 1250 m and 250 m.

Figure 2.12 34

(a) Cross-section of concentration of H_2O_2 in air, cloud, and rain expressed in equivalent gas-phase units (ppbv) at 30 min. simulation time.

(b) Same as 2.12a but at 60 min.

(c) Same as 2.12a but at 90 min. 35

Figure 3.1 52

(a) Liquid water profile for cloud used in delta-Eddington calculation. Representative of rainband at 30 min.

(b) Same as 3.1a but for 60 min.

(c) Same as 3.1a but for 90 min.

Figure 3.2 53

Ozone photolysis rates as a function of height in clear air (dashed line), and in the rainband at 30 min. Curves are identified for Clouds A, B, and C.

Figure 3.3 53

Same as 3.2 but for 60 min.

Figure 3.4 54

Same as 3.2 but for 90 min.

Figure 4.1 67

(a) Vertical cross-section of production rates (ppb/h) of H_2O_2 in cloud at 30 min.

(b) As in 4.1a except at 60 min.

(c) As in 4.1a except at 90 min. 68

(d) As in 4.1a except at 120 min.

Figure 4.2 69

(a) Vertical cross-section of difference between total H_2O_2 (ppbv) in Simulation 2 and total H_2O_2 in the base simulation at 30 min.

(b) As in 4.2a except at 60 min.

(c) As in 4.2a except at 90 min. 70

(d) As in 4.2a except at 120 min.

Figure 4.3 71

Total moles of sulphate formed in cloud and rain by H_2O_2 reaction in the base simulation (solid lines) and Simulation 2 (dashed lines)

Figure 4.4 72

(a) Difference in the concentration of H_2O_2 in cloud (mg/L) between Simulation 2 and the base simulation at 3250 m and 6250 m, vs time.

(b) As in 4.4a except for sulphate in cloud.

Figure 4.5 73

Net change in H_2O_2 (ppb) as a function of height in Simulation 2 (dashed line) and the base simulation (solid line).

LIST OF TABLES

Table 2.1 13
Initial surface concentrations of chemicals
Table 2.2 15
Reactions and solubility constants - from Chameides (1984)
Table 2.3 26
Simulated and measured concentrations of sulphur dioxide in the air, sulphate in air, and sulphate in rain just above and below cloud base.
Table 3.1 43
Gas phase reactions - from Hough (1987)
Table 3.2 47
Coefficients a_i, absorption coefficients K_i, and fraction of F_0 in the wavelength interval $\delta\lambda$.
Table 3.3 48
Rayleigh volume scattering coefficients at T=273 K, p=1013.25 mb - from Penndorf (1957)
Table 3.4 48
Droplet distribution parameters - from Stephens (1979)
Table 3.5 49
Single scattering properties of chosen cloud microphysical models - from Stephens (1979)
Table 3.6 58
Aqueous-phase reactions from Pandis and Seinfeld (1989)
Table 4.1 66
Concentrations from Simulation 2 and measured concentrations of sulphur dioxide in air, sulphate in air, and sulphate in rain just above and below cloud base.

LIST OF SYMBOLS

The following is a list of the principal symbols used in the text and listed in the order that they first appear. For symbols with more than one meaning, the notation is clearly defined where the symbol is used.

Continuity equations:

$Q_{i,a}$	concentration of chemical species i in air (mol/m^3)
ρ_0	density of air (g/cm^3)
$\vec{V}$	total three dimensional wind (m/s)
ν_h	eddy diffusion coefficient (m^2 s^{-1})
$S_{i,a}$	sources and sinks of chemical species i in air (mol/s)

Transfers to aqueous phase:

$[X_{(aq)}]$	concentration of species X in the aqueous phase (M)
H_x	Henry's law constant for species X (M atm^{-1})
p_x	partial pressure of species x in air (atm)
n(x)	concentration of species X in air (cm^3/molecule)
N_{drop}	number of cloud drops per cm^3 of air
$S_r^{\pm}(X)$	source of X to cloud drop of radius r (M s-^{1})
$\phi_r(X)$	rate of transfer of X into and out of a single cloud drop of radius r (molecule/s)
l	mean free path length (cm)
R	universal gas constant (atm m^3 mol^{-1} K^{-1})
m(X)	molecular mass of X (kg)
α	mass accommodation coefficient

δ-Eddington calculation:

$F(\lambda,\theta)$	actinic flux (photons cm^{-2} nm^{-1} s^{-1})
σ_x	absorption cross section of species X (cm^2 $molecule^{-1}$)
$\phi_x(\lambda)$	quantum efficiency of X for reaction
$L(\theta,\phi)$	radiance (photons cm^{-2} nm^{-1} s^{-1} sr^{-1})
f	fraction of scattered radiation in forward peak
g	asymmetry factor
ω	single scatter albedo
τ_i	optical depth due to species i
K_i	absorption coefficient of i
μ	cosine of zenith angle
u	depth of ozone in column (cm (STP))
β_R	Rayleigh volume extinction coefficient
$\langle\cos\theta\rangle$	asymmetry factor
$P(\cos\theta)$	scattering phase function

Reaction rates:

$[M]$	concentration of third body ($molecules/cm^3$)
k_{Gn}	rate constant for nth gas-phase reaction
k_{An}	rate constant for nth aqueous-phase reaction

CHAPTER 1

AN OVERVIEW OF CLOUD CHEMISTRY MODELS

1.1 Introduction

The phenomenon of acid precipitation was identified and discussed as long ago as the middle of the nineteenth century. In 1852, an English chemist identified acid rain in Manchester, England (Seinfeld, 1986). Modern studies, however, have only been since the 1950s and intensive research supported by public awareness really began in the mid-1970s. This widespread concern that acid deposition was creating a serious environmental problem provided the impetus for research in cloud chemistry.

The overall process of acid deposition may be divided into four sub-processes which are: (1) the emission of acid precursors, mostly sulphur dioxide (SO_2) and oxides of nitrogen (NO and NO_2); (2) transport of acids or their precursors by the wind, clear air convection, or clouds; (3) physical and chemical transformation processes such as scavenging of acidic aerosols or oxidation of chemical species; (4) deposition of acids on the earth's surface (Schwartz, 1984a). It was first recognized that clouds and cloud systems could play a significant role in the scavenging, transport, and deposition of acidic species. As more studies of aqueous-phase atmospheric chemistry became available, it became evident that there is a vast and varying number of chemical reactions occurring within the cloud- and rain-droplets themselves.

In midlatitudes, much of the large scale precipitation areas are associated with low-pressure systems (Kreitzberg, 1984). Modelling of these areas is highly complex; much must first be learned from the study of individual clouds or of mesoscale systems that are embedded within the areas. It is on these scales that strong vertical velocities may be found and pollutants may be transported from the boundary layer to higher altitudes where horizontal winds may be more intense. Mesoscale systems, rather than individual clouds, are important to study not only because of their areal extent but they also have longer lifetimes and there is more opportunity for chemical reaction. One mesoscale cloud system that lends itself rather well to a modelling study is the rainband which is an organized line of precipitating clouds. There are different types of rainbands and varying theories for their formation and development exist. Some of these rainbands are lines of convective clouds; others are areas of enhanced precipitation (Cho and Iribarne, 1983). This work will deal with chemical reactions that occur in a convective type rainband - one that forms in the warm sector of a cyclone and is not associated with a frontal system.

There are two basic approaches that help to elucidate the role of clouds in acid deposition. First, there are laboratory experiments for determining thermodynamic and kinetic data and field studies for measuring concentrations of atmospheric chemicals. The information provided by field measurements is necessary for solving the problem but does not provide the whole solution. The direct experimental approach is costly and many times physically impractical. That is where the second approach, that of theoretical studies with mathematical models, proves invaluable.

1.2 Cloud chemistry models

Over the past several years, numerous cloud chemistry models have been developed. The models differ in their degree of elaboration or simplification of dynamical, microphysical, or chemical processes. Generally, the complexity of the chemistry included in the models varies inversely with the complexity of the dynamics and microphysics. The models range from having relatively simple microphysics and dynamics and very detailed chemistry (Seigneur and Saxena, 1984,1988; Chameides, 1984; Hough, 1987) to fully three-dimensional numerical cloud models that include less detailed chemistry (Tremblay and Leighton, 1986; Tremblay, 1987; Niewiadomski, 1989). Although none of these models gives a complete picture of all the physical and chemical processes in clouds, they each provide useful information and have led to some generally accepted conclusions.

Patterns and amounts of acid deposited on the ground are determined by the three processes associated with clouds - microphysics, dynamics, and chemistry. It is useful to examine some of the models that have led to several theories on cloud chemistry.

1.2.1 Chemistry

It is widely recognized that acid precipitation (that with a pH below 5.6, the value of water in equilibrium with CO_2) is mainly caused by the dissolution of sulphuric and nitric acids (H_2SO_4, HNO_3), (Chameides, 1984). While there is no known efficient method of aqueous-phase production of nitric acid, several pathways are considered important for oxidizing sulphur dioxide (SO_2) in cloud droplets (Calvert, 1985). Included in these reaction pathways are oxidations of SO_2 by hydrogen peroxide (H_2O_2), ozone (O_3), organic peroxides (ROOH), and metal-catalyzed oxidation by molecular oxygen.

There have been several detailed chemistry models developed to understand chemical reactions in clouds (Hong and Carmichael, 1983; Jacob and Hoffmann, 1983; Chameides, 1984; Seigneur and Saxena, 1984, 1988; Hough, 1987). Hong and Carmichael, using a flow-through reactor model, considered gas scavenging and aqueous-phase oxidation reactions. They concluded that both H_2O_2 and O_3 could be significant oxidants of SO_2 but the sulphate produced is strongly dependent upon trace gas concentrations. Jacob and Hoffmann (1983) found oxidation by O_2 catalyzed by Fe(III) and Mn(II) to also be significant. They found O_3 oxidation to be important above a pH of 5.0 and the contribution due to H_2O_2 limited because of its depletion. Chameides (1984) used a time-dependent box model with coupled gas- and aqueous-phase chemistry to study the chemistry of a remote stratiform cloud. He suggested the possibility of free-radical reactions in clouds.

Clouds in several different environments were simulated with the box model and later one-dimensional model of Seigneur and Saxena (1984, 1988). Hough (1987) studied the chemistry of different hill clouds in northern England with the use of a one-dimensional model. These researchers investigated the chemical behavior of orographic clouds resulting from the lifting of airmasses with differing histories. In each of these models, microphysical and dynamic processes were highly parameterized but very detailed gas- and aqueous-phase reactions were included. The results clearly demonstrate that different oxidation mechanisms are important in different types of clouds, at different times, and under different pollutant loadings.

1.2.2 Microphysics

Among the models that have demonstrated the importance of scavenging of pollutants by clouds and precipitation particles are Scott (1978), Hales (1982), and Flossmann et al. (1985). Hales (1982) included scavenging of sulphate aerosol by nucleation and scavenging of $SO_{2(g)}$ in a one-dimensional, time-variant model. He suggested that in-cloud scavenging is dependent on aerosol particle size. Flossmann et al. (1985) modelled the time evolution of a drop size distribution forming on a given aerosol spectrum. Among their conclusions are: (1) the importance of nucleation scavenging relative to impaction scavenging; (2) the higher contamination of small drops as compared to larger ones.

Flossmann et al. (1987) extended the earlier model to include a parameterized oxidation mechanism as well as scavenging of gaseous SO_2 and ammonium sulphate $[(NH_4)_2SO_4]$ particles by cloud and precipitation drops. Their model showed the effect of a condensation/evaporation cycle on a given aerosol spectrum. For their particular case, the particle distribution became broader implying an increased number of potential cloud condensation nuclei for a second cloud cycle. Flossmann et al. (1987) found the sulphur concentration in large cloud drops to be greater than in small drops because of the longer age of the large drops. This in turn implies a lower pH in large drops than in small. These results contrast with those of Lee (1986). Lee's results give lower pH values for small drops. He suggests that the dilution by liquid water overcompensates for the increase in uptake of acidic species.

The numerical model of Hegg et al. (1984) included nucleation and impaction as well as oxidation of SO_2. It is based on the two-dimensional kinematic, warm-frontal precipitation model of Rutledge and Hobbs (1983). (Their model includes ice and snow as well as liquid water and water vapour.) The cloud chemistry includes scavenging of sulphate particles as well as oxidation of SO_2 by steady concentrations of H_2O_2 and O_3. Their results indicate the importance of cloud microphysical processes in determining sulphate deposition. The dominant mechanism for incorporating SO_4^{2-} into the cloud and rain was found to be nucleation.

Studies of the micropyhsics and chemistry of cold-frontal rainbands (Rutledge et al., 1986; Hegg et al., 1986) followed the study of Hegg et al. (1984). The chemistry model was extended to include scavenging of nitric acid and PAN (peroxyacetyl nitrate). Unlike Hegg et al. (1984), peroxide was not kept constant throughout the simulation but could be depleted by reaction with aqueous S(IV). They found H_2O_2 to be the main oxidant of S(IV) in solution and that sulphate production was not a linear function of sulphur input or H_2O_2 concentration.

1.2.3 Dynamics

In the simulations of Hegg et al. (1986), it was also found that variations in cloud dynamics and microphysics could produce changes as significant as those changes caused by varying the chemical inputs over realistic ranges. It is known that the air motions associated with clouds can redistribute pollutants vertically thus moving pollutants from the boundary layer to the free troposphere. Tremblay and Leighton (1984) and Walcek and Taylor (1986) used one-dimensional models of cumulus clouds. Lee (1986), with a two cylinder model, identified areas in cloud and in near-cloud air where there was a reduction of SO_2 due both to air movements and chemical reactions.

Tremblay and Leighton (1986), Tremblay (1987), and Niewiadomski (1986, 1989) studied cloud-pollutant interactions with three-dimensional numerical cloud models. With these more complete dynamic models, effects of entrainment or turbulent mixing could better be represented. Niewiadomski found that pollutant concentrations equivalent to those in the boundary layer could be found at cloud top. This resulted in a large horizontal variability in pollutant concentrations across a field where there was cumulus convection. Tremblay and Leighton found significant transport of SO_2 during the cloud lifetime.

1.3 Modelling aqueous-phase H_2O_2 production

The diversity of existing cloud chemistry models has been shown as well as some of the knowledge gained from them. There are, nevertheless, areas that need further study. Although hydrogen peroxide and ozone are widely considered to be the major oxidants of SO_2 in the aqueous phase, the relative importance of the two oxidants depends to a great deal on the amount of H_2O_2 available for reaction. The oxidation of SO_2 by H_2O_2 is a fast reaction and dominates below a pH of approximately 5.0. But as the reaction proceeds, the importance of H_2O_2 decreases as its concentration diminishes. Several groups have measured gas- and aqueous-phase concentrations of H_2O_2. Measurements of aqueous-phase H_2O_2 range from 10^{-5} - 10^{-4} moles/litre (Kok, 1980; Zika et al., 1982; Daum et al., 1984; Kelly et al., 1985). These values are consistent with the theoretical concentration of gaseous H_2O_2 being in the range of 0.1 to 1 ppb (parts per billion). It is only recently that gas-phase H_2O_2 has been measured directly and these results will help to clarify the role of peroxide in the troposphere. Heikes et al. (1987) measured tropospheric gas-phase concentrations from the eastern United States in autumn to be 0.2 - 4.1 ppb with maximum concentrations found just above cloud top. Winter measurements are reported by Barth et al. (1989) from flights off North and South Carolina and are generally less than 1 ppb with a maximum of 2.4 ppb. Isaac et al. (1988), in preliminary results of their summer field study near Muskoka, Ontario, showed H_2O_2 measurements ranging from about 1.5 - 4.5 ppb.

In most aqueous-phase models, peroxide is assumed to come from the dissolution of $H_2O_{2(g)}$ from the cloud interstitial air. Observations by Zika et al. (1982) indicated that during some rain events H_2O_2 appeared to be produced within the cloud. These observations led to several modelling studies that examined the possibility of in-cloud H_2O_2 production (Chameides and Davis, 1982; Schwartz, 1984b; Chameides, 1984; Seigneur and Saxena, 1984; Walcek, 1988; Pandis and Seinfeld, 1989). A source of $H_2O_{2(aq)}$ that has been included in some models is the reaction of the superoxide ion, O_2^-, with the bicarbonate ion, HCO_3^-. There exists some debate over this reaction. Schwartz (1984b) has concluded that it is unimportant in cloud water since it is exactly compensated for by the reverse reaction. The reaction of two hydroperoxy radicals (HC_2), scavenged from the gas phase, has also been examined. Chameides and Davis (1982), Schwartz (1984b), and Chameides (1984) found that the scavenging of HO_2 radicals from the gas phase by cloud droplets could be an important source of H_2O_2 in cloud. Seigneur and Saxena (1984) found that under high sun conditions, formation of H_2O_2 could exceed its rate of consumption in cloud. Walcek (1988) included H_2O_2 production in a cloud updraft model. He found that near cloudtops, H_2O_2 production rates could be 0.5 ppb per hour. Some uncertainty in early calculations was the rate at which the radicals could be scavenged relative to the rate at which they would be lost to gas-phase reactions. Experimental results of Mozurkewich et al. (1987) suggest that the scavenging rate could be fast enough to warrant the consideration of aqueous-phase reactions.

1.4 Purpose of thesis

The purpose of this thesis is to examine the effects of in-cloud production of H_2O_2 on the oxidation in a rainband with the use of a numerical model. The model is a two-dimensional version of the Tremblay-Leighton cloud chemistry model and has been used by Pitre (1986) and Giles (1987). The chemistry of this specific rainband has been studied by Pitre (1986). The second chapter of this thesis contains a description of the cloud chemistry model and a description of the simulation with no H_2O_2 production. This simulation was first carried out by Pitre. The chemistry of this run has been re-evaluated after some changes have been made to the model (these corrections will be further discussed in Chapter 2). In Chapter 3, the formation of H_2O_2 by the hydroperoxy radical (HO_2) will be discussed. Here, the gas-phase production of HO_2 in the troposphere along with the transfer of radicals into the aqueous-phase will be reviewed. Because the production of HO_2 radicals is initiated by a photochemical process, the calculation of the ultra-violet radiation available in the rainband is also presented. Chapter 4 will present results of the simulation that includes the in-cloud H_2O_2 source and will discuss the effect of this source on the chemistry of the rainband. Chapter 5 will include some conclusions as regards the simulations. Possible implications to different systems will be discussed as well as limitations of the parameterization method.

CHAPTER 2
BASE SIMULATION

2.1 Introduction

The model used in this study is a version of the cloud chemistry model developed by Tremblay and Leighton (1986). It was reduced to two dimensions and used to study the chemistry of a warm rainband (Pitre, 1986). Giles (1987) extended the model to include the ice phase but found no significant changes in the chemistry when snow and ice were included. The combination of two numerical models simulates the solution-phase chemistry and the detailed dynamics and microphysics of a rainband. The models are uncoupled under the assumption that the cloud chemistry does not affect the rainband dynamic and microphysical processes. As input at each timestep, the chemistry model requires horizontal and vertical wind fields, atmospheric water, and effects of mixing along with information about condensation and evaporation. The dynamical model provides these fields but it is not necessary for the two models to be run simultaneously. The output from the dynamic model can be stored and later read by the chemistry model. The use of the models in this manner, provides an efficient use of computer time without sacrificing detail.

The domain simulated is 500 km in the x-direction and 12 km in the vertical; a single grid point models the y-direction. This domain represents a vertical section of the rainband oriented in a direction perpendicular to the rainband axis and parallel to the direction of motion. The use of two dimensions, instead of three, assumes that this domain is representative of any cross-section along the y-axis. The vertical grid spacing is 500 meters but a stretched coordinate system is employed for the x-axis (included by Valton, 1986). In this coordinate system, the horizontal grid spacing varies from 18 km at the edges of the domain to approximately 1 km at the centre. The rainband is maintained in the region of highest resolution at the centre of the domain by subtracting the mean horizontal wind from the total wind field.

The simulation to be used as a base for determining the importance of H_2O_2 production will be described in this chapter. It is based on the work of Pitre (1986) with several changes made to the model: (1) A temperature dependence for the reactions was included as in Chameides (1984); (2) The Henry's law constant for ozone dissolving in water was corrected to a value of 1.15×10^{-2} M atm^{-1} at 298 K (Chameides, 1984); (3) Determined to be more appropriate for the oxidation of S(IV) by O_3, the rate expression of Maahs (1983) replaces that of Martin (1983); (4) At high pH (>5.5), it was found that a 15 second timestep was too long for the fast S(IV)-O_3 reaction and a weighted average oxidation rate based on a variable timestep was used.

2.2 Chemistry model

2.2.1 Continuity equations

The chemistry model is similar to the dynamics model in its domain, grid spacing, and use of stretched coordinates. As mentioned earlier, the chemistry model can simply read the necessary fields from magnetic tape at each timestep. For each chemical, continuity equations are solved which describe its redistribution, phase transitions, and chemical reactions. A sample continuity equation for a species i in air is as follows:

$$\begin{aligned} \frac{\partial}{\partial t} Q_{i,a} = & - \rho_0^{-1} \nabla \cdot (\rho_0 Q_{i,a} \vec{V}) \\ & + \rho_0^{-1} \nabla \cdot [\nu_h \rho_0 \nabla (Q_{i,a}^{t=n} - Q_{i,a}^{t=0})] \\ & + S_{i,a} \end{aligned} \qquad (2.1)$$

The terms on the right of the equation represent the advection of species i by the total wind, the diffusion of i, and the various sources and sinks of i. The diffusion scheme used in the model is base-state diffusion, in which pollutants diffuse with respect to their base states. Pitre (1986) found that a regular diffusion scheme which transports chemicals down gradient, caused pollutants in areas outside the area of convection to be strongly diffused upwards. This transport was contrary to the observations which suggested that initial profiles were being maintained by some large scale forcing and the addition of the base-state diffusion scheme corrected the problem in these areas. The equations for i in the cloud and rain are analogous to (2.1) with a term added to the rain equation to correct the vertical advection of i due to the terminal fallspeed of the rain.

2.2.2 Chemical species modelled

The focus of the model is aqueous phase sulphur chemistry. Sulphur species included are sulphur dioxide (SO_2) and a sulphate aerosol which is a mixture of sulphuric acid (H_2SO_4) and ammonium sulphate ($(NH_4)_2SO_4$). In the model, SO_2 may be oxidized by hydrogen peroxide (H_2O_2) or ozone (O_3). Nitric acid (HNO_3), ammonia gas (NH_3), and carbon dioxide (CO_2) are included for their effect on pH.

The initial concentrations of the chemical species are given in Table 2.1. The concentrations of SO_2, HNO_3, NH_3, and sulphate aerosol have a maximum concentration at the ground and decrease exponentially with height. A first simulation was studied in which a similar profile was assumed for H_2O_2 but in light of measurements reported by Heikes et al. (1987), Barth et al. (1989), and Isaac et al. (1988) this profile seemed inappropriate for a summer or autumn study. A vertically uniform initial profile seemed a better approximation and accordingly all results presented here are for this profile. The concentrations of CO_2 and O_3 were both uniform and constant throughout the simulation.

Table 2.1 Initial surface concentrations of chemicals.

Chemical	Concentration
HNO_3 *	0.3 ppb
SO_2 *	4.0 ppb
NH_3 *	1.5 ppb
SO_4^{2-} *	12.92 $\mu g/m^3$
H_2O_2	1.0 ppb
O_3	50 ppb
CO_2	330 ppb

* concentration drops off with a scale height of 900 m

2.2.3 Solubility constants and aqueous-phase equilibria

All of the chemicals may exist in air, cloud, or rain. Gases are assumed to be in thermodynamic equilibrium with the species dissolved in cloud as described by Henry's law. This law states that for dilute solutions, there is a linear relationship between the concentration of a gas dissolved in a liquid and the partial pressure of the gas above the solution. For example, the equilibrium concentration of a species X would be given by:

$$[X_{(aq)}] = H_X \, p_X$$

where H_X is the Henry's law coefficient and p_X is the partial pressure of X. For a chemical such as SO_2, undergoing rapid aqueous-phase equilibria, an effective Henry's law coefficient must be employed to include the total dissolved species.

The dissolution of gaseous SO_2 and subsequent aqueous-phase equilibria are described by the following equations:

$$SO_{2(g)} \leftrightarrow SO_{2(aq)}$$

$$SO_{2(aq)} \leftrightarrow HSO_3^- + H^+$$

$$HSO_3^- \leftrightarrow SO_3^{2-} + H^+$$

Sulphur in the +4 oxidation state, S(IV), is the sum of $SO_{2(aq)}$, bisulphite (HSO_3^-), and sulphite (SO_3^{2-}). The aqueous concentration of S(IV) is related to gaseous SO_2 by the effective Henry's law constant, $H_{s(IV)}$, defined as:

$$H_{S(IV)} \equiv [S(IV)] \,/\, p_{SO_2}$$

$$= ([SO_{2(aq)}] + [HSO_3^-] + [SO_3^=]) \,/\, p_{SO_2}$$

$$= H_{SO_2} \; (1 + k_1/[H^+] + k_1 k_2/[H^+]^2)$$

where k_1 and k_2 are the first and second ionization constants of sulphurous acid (Schwartz, 1986).

Values of the solubility constants are given in Table 2.2 and are from Chameides (1984). Highly soluble gases like NH_3 and HNO_3 are assumed to dissolve completely in cloud and to be irreversibly scavenged by rain. Hydrogen peroxide is in equilibrium with H_2O_2 dissolved in cloud and is assumed to be irreversibly scavenged by rain. Sulphur dioxide is in equilibrium with S(IV) in cloud and rain. Finally, O_3 and CO_2 are considered in equilibrium and because of their high gas-phase concentrations and low solubility, their gas-phase concentrations are maintained at constant values.

Table 2.2 Reactions and solubility or equilibrium constants. Chameides (1984)

Reaction	Solubility / equilibrium constant
$HNO_{3(g)} \leftrightarrow H^+ + NO_3^-$	$2.6\text{x}10^{6} \exp\left[8700\left(\frac{1}{T} - \frac{1}{298}\right)\right]$ $M^2\,atm^{-1}$
$NH_{3(g)} \leftrightarrow NH_{3(aq)}$	$5.8\text{x}10^{1} \exp\left[4085\left(\frac{1}{T} - \frac{1}{298}\right)\right]$ $M\,atm^{-1}$
$SO_{2(g)} \leftrightarrow SO_{2(aq)}$	$1.23 \exp\left[3120\left(\frac{1}{T} - \frac{1}{298}\right)\right]$ $M\,atm^{-1}$
$CO_{2(g)} \leftrightarrow CO_{2(aq)}$	$3.11\text{x}10^{-2} \exp\left[2423\left(\frac{1}{T} - \frac{1}{298}\right)\right]$ $M\,atm^{-1}$
$O_{3(g)} \leftrightarrow O_{3(aq)}$	$1.15\text{x}10^{-2} \exp\left[2560\left(\frac{1}{T} - \frac{1}{298}\right)\right]$ $M\,atm^{-1}$
$H_2O_{2(g)} \leftrightarrow H_2O_{2(aq)}$	$9.7\text{x}10^{+4} \exp\left[6600\left(\frac{1}{T} - \frac{1}{298}\right)\right]$ $M\,atm^{-1}$
$SO_{2(aq)} \overset{H_2O}{\leftrightarrow} HSO_3^- + H^+$	$1.7\text{x}10^{-2} \exp\left[2090\left(\frac{1}{T} - \frac{1}{298}\right)\right]$ M
$HSO_3^- \leftrightarrow H^+ + SO_3^=$	$6\text{x}10^{-8} \exp\left[1120\left(\frac{1}{T} - \frac{1}{298}\right)\right]$ M
$NH_3 \overset{H_2O}{\leftrightarrow} NH_4^+ + OH$	$1.7\text{x}10^{-5} \exp\left[-4325\left(\frac{1}{T} - \frac{1}{298}\right)\right]$ M

2.2.4 Oxidation reactions

Two reactions are included that can oxidize S(IV) to S(VI). These are:

$$S(IV) + O_3 \rightarrow S(VI) + O_2 \qquad \text{RA2.1}$$

$$S(IV) + H_2O_2 \rightarrow S(VI) + H_2O \qquad \text{RA2.2}$$

The rate expression for RA2.1 is from Maahs(1983).

$$\frac{d}{dt}[S(VI)] = k_{RA2.1}[O_3]\,[S(IV)]$$

where:

$$k_{RA2.1} = \left[4.4\text{x}10^{11}\exp\left(\frac{-4131}{T}\right) + \frac{2.6\times10^{+3}\exp(-966/T)}{[H^+]}\right]$$

For the pH range of interest (3.0-7.0), it is considered to be an appropriate rate (Hoffmann, 1986). The rate expression previously used in the model was that given by Martin (1983). A comparison of the two rate constants is given by Figure 2.1. The two rates agree at a pH of 3.0 but differ by as much as a factor of 20 at pH 6.0 and 298K.

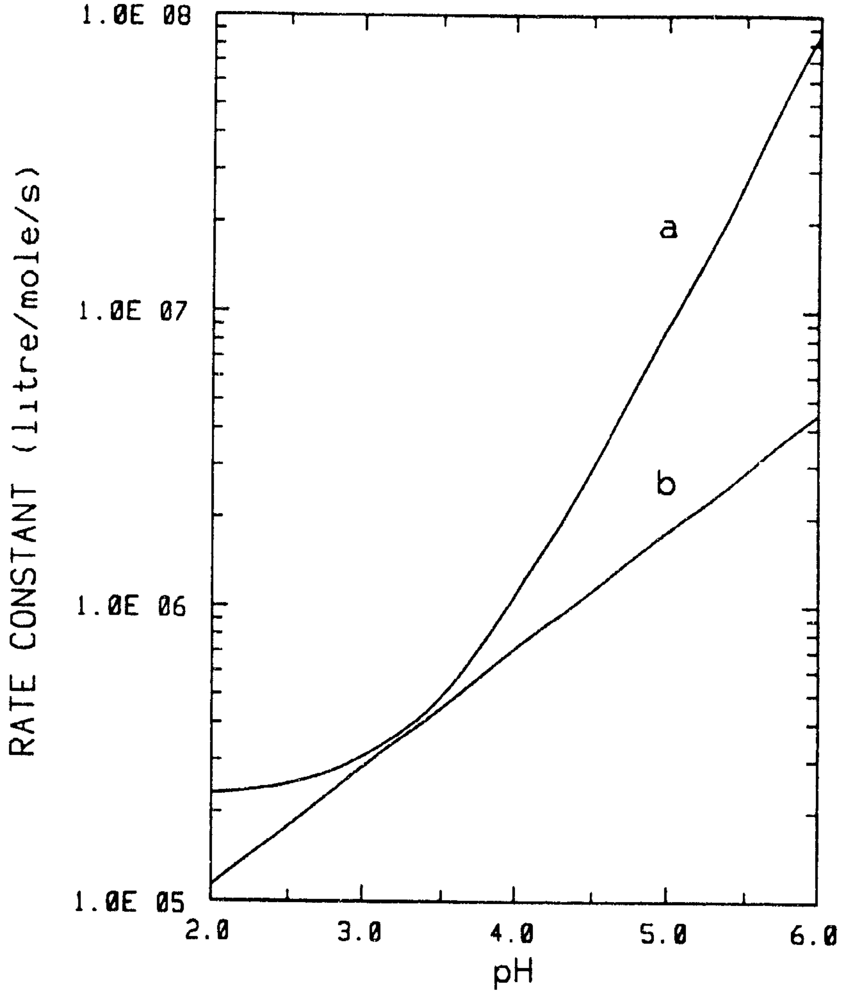

Figure 2.1 Comparison of rate constants as a function of pH for oxidation of S(IV) by O_3. (T = 298 K). Rate constants from (a) Maahs (1983)
(b) Martin (1983)

The rate expression for RA2.2 is from Martin (1983) and is given as:

$$\frac{d}{dt} [S(VI)] = k_{RA2.2} [H_2O_2] [S(IV)]$$

where:

$$k_{RA2.2} = \frac{8.0\times10^4}{(0.1 + [H^+])} \exp\left[-3650 \left(\frac{1}{T} - \frac{1}{298}\right)\right]$$

The fractional rates of reaction for RA2.1 and RA2.2 at 285 K are shown in Figure 2.2. The solubility of SO_2 decreases with pH but the rate constant of RA2.2 increases and thus a near independence of pH in reaction rate. The rate of RA2.1 is very fast at high pH but is highly pH dependent. In fact, the O_3 rate is self-limiting; as SO_4^{2-} is produced, the pH decreases and the reaction rate decreases. At high pH, the reaction rate could not be assumed constant over the timestep of the model. For example, at a pH of 6.0 and temperature of 285 K, more than 100% of the S(IV) dissolved in cloud is oxidized in one timestep. To use a timestep small enough for this reaction at high pH would be computationally prohibitive. Instead, at a pH greater than 4.5, the model incorporates a variable timestep for the solution of RA2.1 to approximate the self-limiting behavior of the O_3 reaction rate.

Timesteps are varied in three pH ranges. For pH≤4.5, a 15 second timestep is adequate. In the pH range 4.5-5.4, a 1.0 second timestep is used and between pH=5.4 and pH=6.0 a 0.1 second timestep is needed. The moles of sulphate produced over the total 15 seconds result from a weighted average oxidation rate.

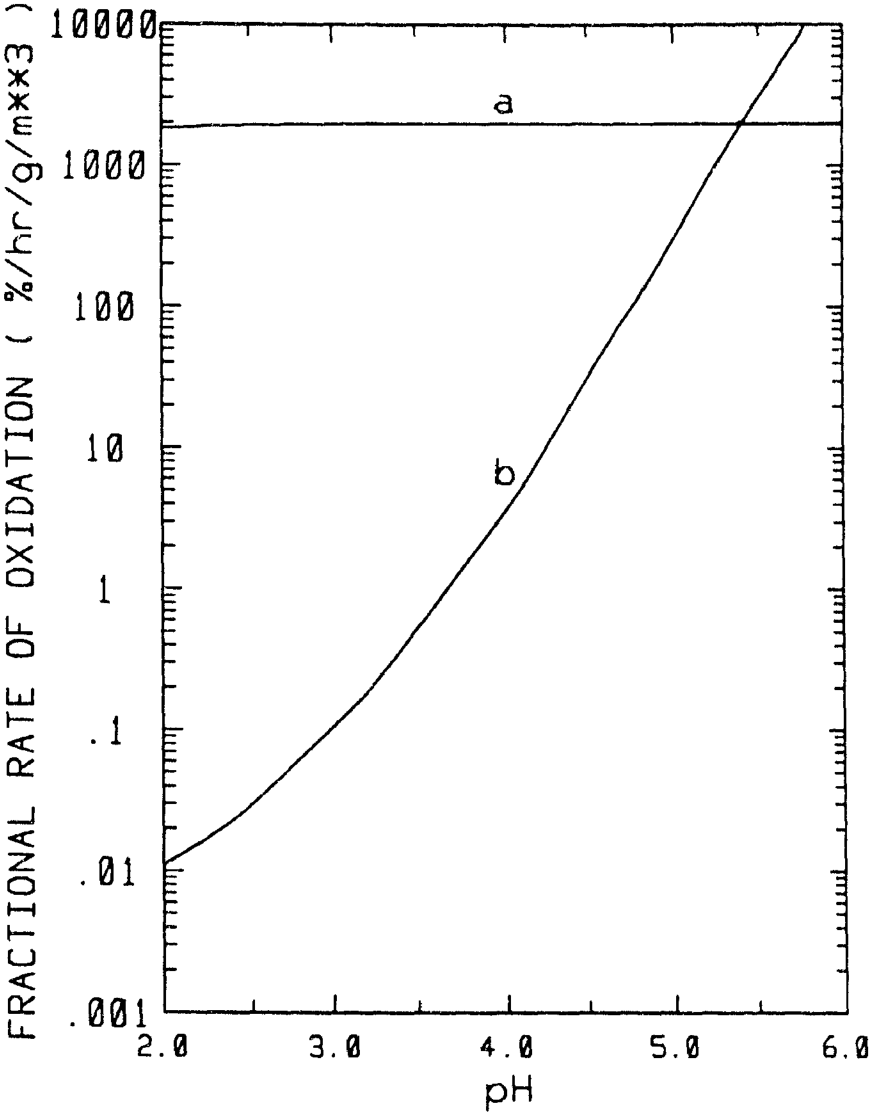

Figure 2.2 Fractional rate of oxidation of S(IV) by (a) 1 ppb H_2O_2, (b) 50 ppb O_3, vs solution pH (T = 285 K).

2.3 Results of base simulation

2.3.1 Dynamics

The dynamic fields used as input were obtained from a simulation of a rainband that formed over southern Ontario on November 5, 1981. This rainband was extensively studied by Isaac et al. (1983) and Chang (1984). The characteristics of the dynamics model simulation are fully discussed in Valton (1986), Pitre (1986), and Giles (1987) and will not be discussed in depth here. There are, however, several features that should be restated. Pitre noted five phases of the rainband:

(1) 0-15 min - cloud development

(2) 15-50 min - development of three distinct cells and formation of rain

(3) 50-90 min - depletion of rainband at leading and trailing edges and formation of a large central cell

(4) 90-120 min - 'steady state' phase, no additional growth or decay

(5) 120-180 min - decay of rainband

Figure 2.3 shows the cloud boundary and rainwater concentration at 90 minutes. Two distinct rainshafts can be seen. It is at this time that the simulated rainband most closely resembles the observed rainband.

2.3.2 Sulphate in cloud and rain

(a) Nucleation and scavenging of sulphate

Sulphate can enter the cloud through nucleation of sulphate aerosol or be formed in cloud by oxidation of SO_2. The sulphate budget of the cloud is shown in Figure 2.4. Nucleation and oxidation contribute sulphate in a ratio of 4:1. Of the total moles of SO_4^{2-} that enters cloud, approximately 22 percent is transferred to rain; the majority (approximately 76 percent) returns to air through

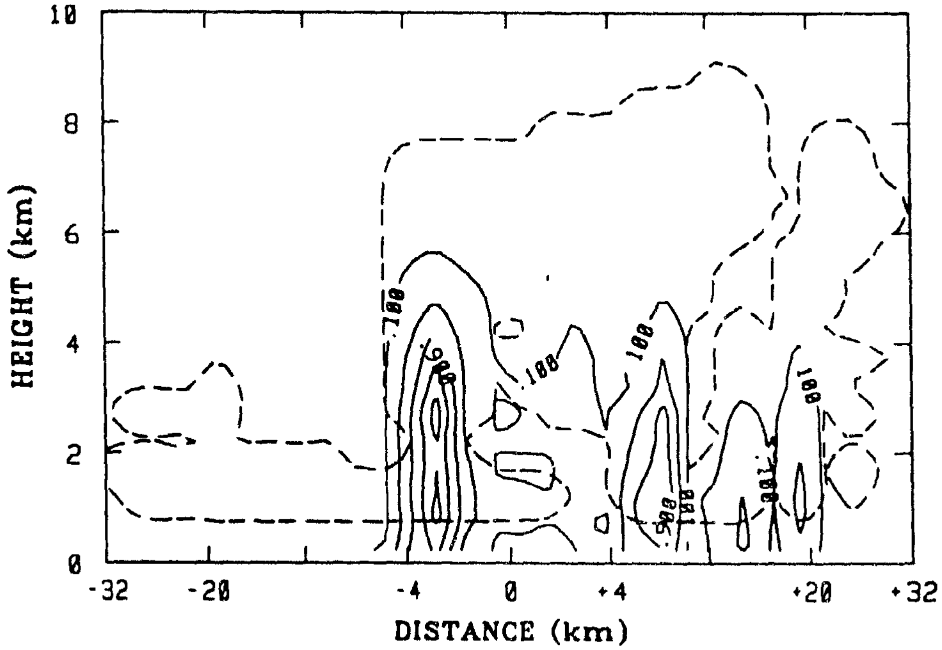

Figure 2.3 Vertical cross-section of rainwater concentration at 90 minutes simulation time. Contour interval is 0.4 g/m^3. Broken line denotes cloud boundary.

evaporation of cloud.

In rain, scavenging of sulphate aerosol provides 38 percent of the total sulphate. The contributions from collection of cloud drops and in-rain oxidation are 36 and 26 percent respectively (Figure 2.5). The importance of oxidation in cloud to the total moles of sulphate transferred from cloud to rain can be inferred from comparison of the transfers from cloud to rain shown in Figure 2.5. A sensitivity test was performed in which there was no in-cloud oxidation. The transfer in this run is shown as the dashed line and it can be seen that the moles of sulphate transferred from cloud to rain were reduced by about 30 percent.

(b) Oxidation of SO_2

Sulphur dioxide is oxidized in cloud and rain by H_2O_2 and O_3. Hydrogen peroxide is the dominant oxidant and its depletion tends to limit the overall oxidation. Approximately 74% of the total sulphate produced during the simulation is by the peroxide reaction. The relative importance of H_2O_2 and O_3, however, differs from cloud to rain.

Moles of sulphate formed in cloud and rain by H_2O_2 and O_3 reactions are given in Figure 2.6. There are several points to note about this figure. More than half of the sulphate formed in cloud is within the first 35 minutes of the simulation. In cloud, H_2O_2 accounts for 84% of the sulphate produced while in rain it is 62%. This difference can be attributed to two major factors: (1) When the rain forms at 30 minutes, there is less H_2O_2 available for reaction; (2) The pH values of the rain are slightly higher than in cloud thus favouring the ozone reaction.

The reduction in the oxidation rate in cloud and rain as the simulation progresses is clearly demonstrated in Figures 2.7a, b where the total rates of sulphate production are plotted as a function of simulation time. In cloud

(Figure 2.7a), there is a marked decrease in SO_4^{2-} production by reaction with H_2O_2 during the first 30 minutes. The rate of sulphate production in cloud due to ozone remains relatively constant. In rain (Figure 2.7b), the total rate of oxidation of S(IV) by H_2O_2 is maintained for approximately 30 minutes as rain falls below cloud base and scavenges SO_2 and H_2O_2.

Oxidation rates at different levels in cloud can be compared. Figure 2.8a gives the total rate of SO_4^{2-} production (moles/s) by H_2O_2 across the rainband at cloud base (1250 m) and 1 km above cloud base. A greater decrease in the rate of oxidation by H_2O_2 is seen at 2250 m than at cloud base. This rate decrease is caused by the depletion of H_2O_2. Figure 2.9 gives the concentration of H_2O_2 dissolved in cloud at 1250 and 2250 m in units of milligrams per litre. The depletion of peroxide is more pronounced at 2250 m; at 1250 m, there is some H_2O_2 being replaced by advection of H_2O_2 from below cloud base. Total rates of oxidation by O_3 at 1250 m and 2250 m are shown as a function of time in Figure 2.8b and may be compared with those in Figure 2.8a. Oxidation of S(IV) by ozone remains approximately constant throughout the simulation and appears to be less important than H_2O_2 at all levels throughout the cloud. It is only at the end of the simulation that the O_3 and H_2O_2 rates become similar. This is due not only to the depletion of $[H_2O_{2(aq)}]$ but also to an increase in the cloud pH (Figure 2.10) and thus a slight increase in the ozone rate.

Unlike cloud, H_2O_2 reaction in rain does not dominate at all levels. Total in-rain oxidation rates at different levels are shown in Figures 2.11a, b. Below cloud base, where much of the in-rain oxidation occurs, there is more H_2O_2 available for reaction and its contribution to SO_4^{2-} is most important. Higher in the rainband, O_3 and H_2O_2 make comparable contributions.

The decrease of total H_2O_2 in the domain can be seen in

Figures 2.12a, b, c. These figures show the total peroxide in air, cloud, and rain across the rainband expressed in equivalent gas-phase values at three times during the simulation. Equivalent gas-phase units are as if all the peroxide in the domain were transferred to air. At 30 minutes, the oxidation has occurred at low levels in the rainband and almost uniformly across the domain. At 60 minutes, a substantial reduction in peroxide can be seen in regions of updraft as SO_2 has been advected up into higher regions in the domain. At this time, 70 percent of the peroxide lost from the domain is lost to oxidation reactions - 30 percent being removed by rain. By 90 minutes, the total peroxide has been reduced by a factor of about 5 throughout the whole cell.

(c) Comparison with observations

Finally, because the rainband simulated was also the subject of a field study, a comparison can be made between observations and model results (Table 2.3). Although it is necessary that comparisons be made to validate the model results, the limits of these comparisons must also be recognized. Overall, agreement between observations and model results is reasonably good.

The concentrations of sulphate in rain below cloud base agree quite well with observations; the simulated values are about 30% too low. The concentrations in air have not changed much from the initial values and are about 55% higher than the observed values. Because it was found that only about 35% of the sulphate in rain came from oxidation processes (26% from rain, 9% from cloud), a large error could be made in the initial SO_2 field to still yield good results of SO_4^{2-} in the rain. The accuracy of the initial aerosol profile is more important in this case. It is found that the initial SO_2 and the simulated concentrations of SO_2 in air are less than the value quoted as observed in the band. The values of SO_2 in the lower levels of the domain are relatively unchanged throughout the simulation being kept close to their initial values. It is not apparent why the concentrations at these levels should increase as is seemingly indicated by observations - SO_2 should be advected upwards in the domain and also should be lost to reaction. Possibly the inicial profile of SO_2 is too low.

The values from the simulation represent concentrations that have been averaged across the rainband. The SO_2 observed concentrations from the rainband traverse at 875 mb varied considerably from a maximum of approximately 15.8 µg/kg in the leading portion to about nil near the tail of the band. At 815 mb the values range from 5.0 - 11.4 µg/kg, the maximum occurring in the centre of the band. These numbers are noted to stress the variability in measurements and the caution that is required in making comparisons between model results and field observations.

There are several aspects of the base simulation that support its use as a starting point for further study. First, the relatively good agreement between model results and observations is encouraging. In spite of the uncertainties inherent in both the model output and the observations, the two agree quite well. Although the results are sensitive to the initial concentrations of chemicals, it should be noted that initial profiles were also obtained from observations. The initial profile of H_2O_2 was not measured in the field study and does differ from the profile used in a first simulation. In recent years, however, as vertical profile data of gas-phase H_2O_2 have become available, the use of a vertically uniform profile of H_2O_2 seems reasonable. Second, the SO_4^{2-} concentrations err on the low side which supports the search for additional sources of sulphate in cloud and rain. And third, the dominant oxidant in the simulation is H_2O_2 but its rapid depletion limits the rate of oxidation in cloud and rain. It is from this point that additional sources of H_2O_2 to cloud and rain can be considered.

Table 2.3 Simulated and measured concentrations of sulphur dioxide in the air, sulphate in air, and sulphate in rain just above and below cloud base. Numbers in parenthesis are maximum and minimum measured values

Time (min.)	$[SO_2]_a$ (μg/kg)	$[SO_4^{=}]_a$ (μg/kg)	$[SO_4^{=}]_r$ (mg/L)
1250 m			
Observed	5.0	2.6	2.2
	(1.6-11.4)	(0.7-5.6)	
90	1.85	3.92	1.21
100	1.78	3.95	0.94
110	1.69	4.03	0.93
120	1.61	4.13	0.78
750 m			
Observed	7.3	4.0	1.8
	(0.0-15.8)	(0.6-9.0)	
90	3.96	6.59	1.58
100	3.87	6.60	1.30
110	3.78	6.63	1.26
120	3.69	6.64	1.06

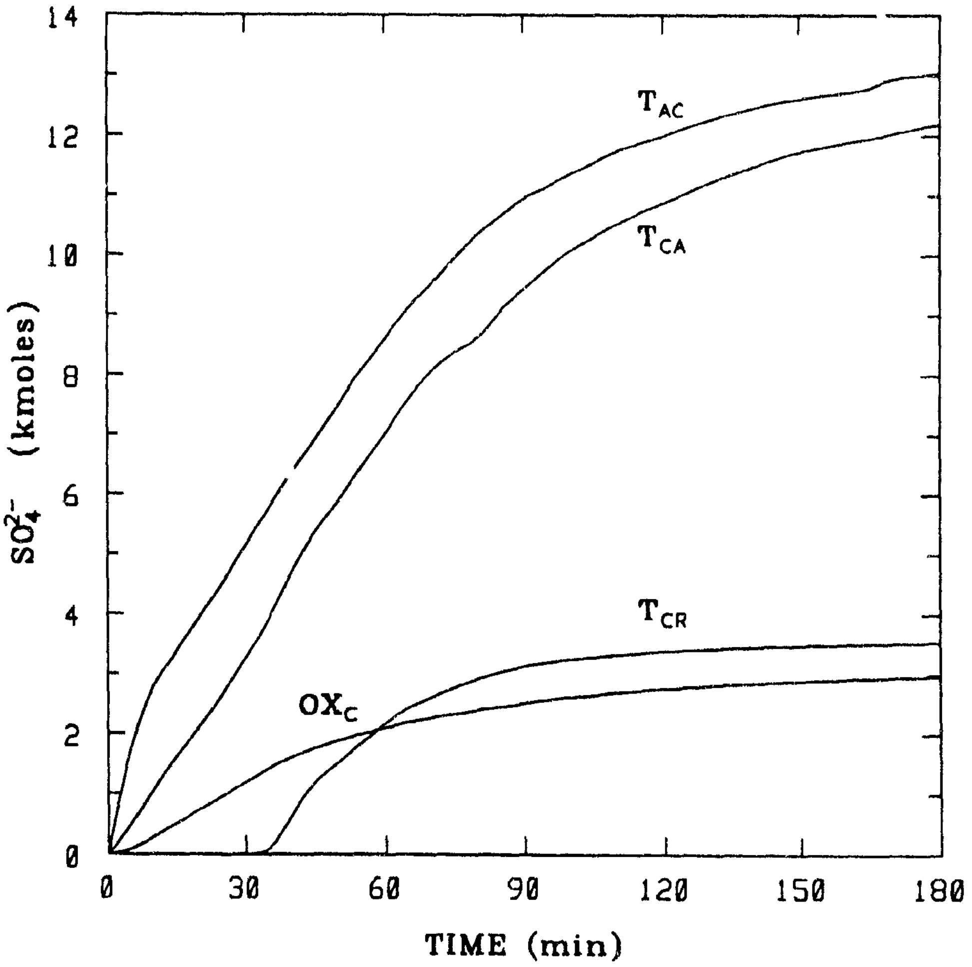

Figure 2.4 Cloud sulphate budget: Moles of sulphate transferred from air to cloud (T_{AC}), cloud to air (T_{CA}), cloud to rain (T_{CR}). Sulphate formed in cloud by oxidation mechanism is OX_C.

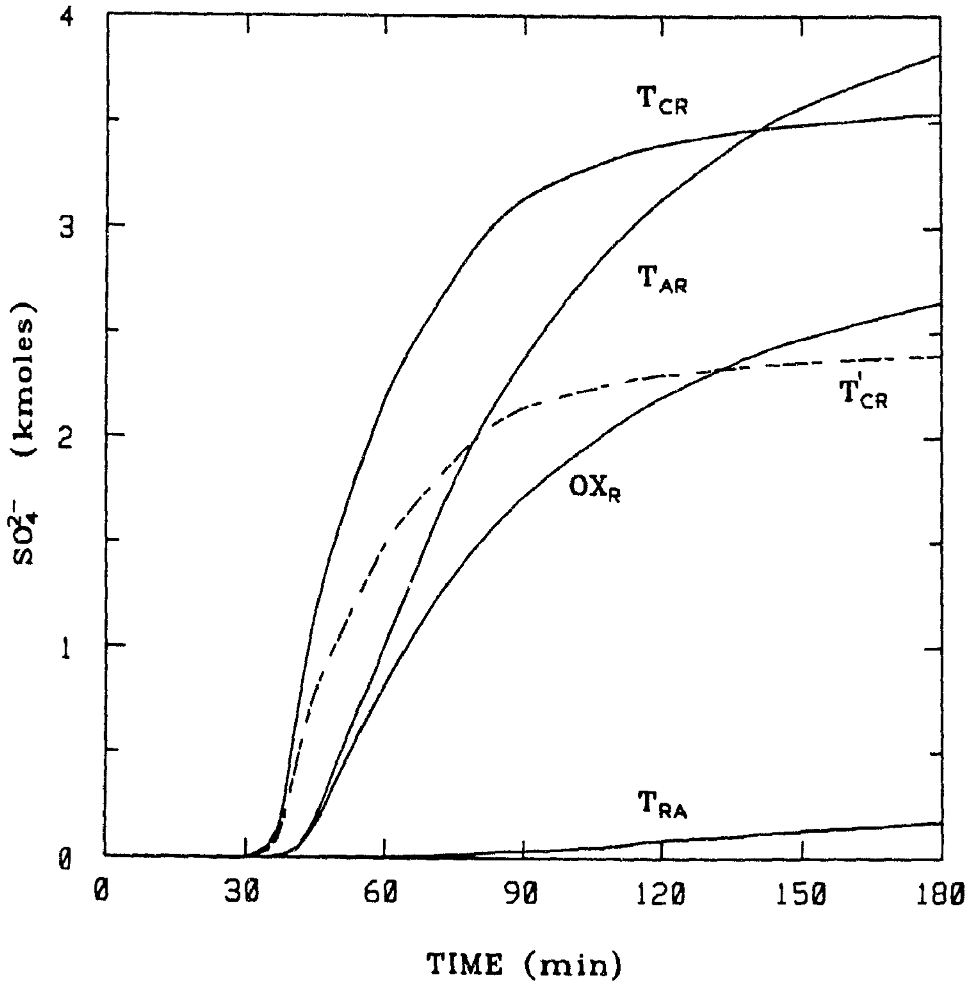

Figure 2.5 Rain sulphate budget: Moles of sulphate formed in rain (OX_R) during simulation and transfers of sulphate involving rain. T_{CR} - cloud to rain T_{RA} - rain to air, T_{AR} - air to rain. T'_{CR} is sulphate transferred cloud to rain during simulation with no in-cloud oxidation.

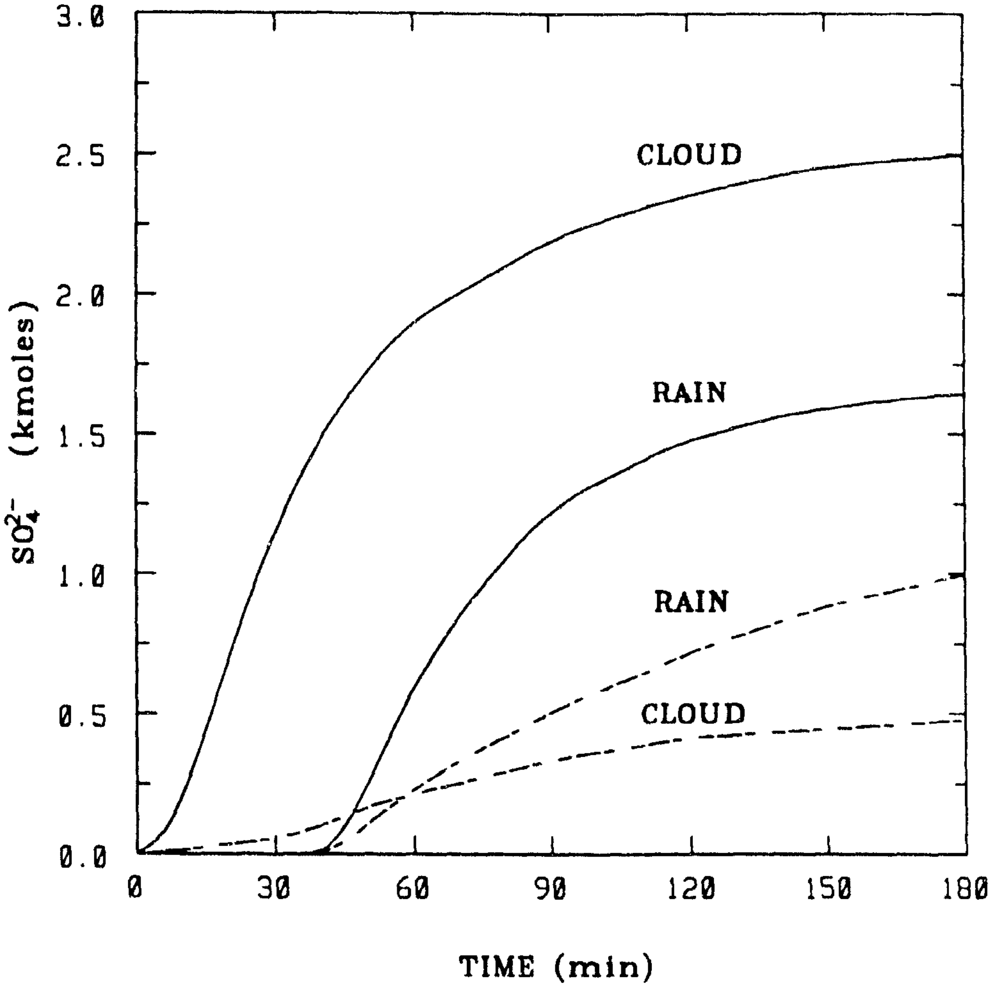

Figure 2.6 Total moles of sulphate formed in cloud and rain by oxidation of S(IV) by H_2O_2 (solid lines) or O_3 (dashed lines).

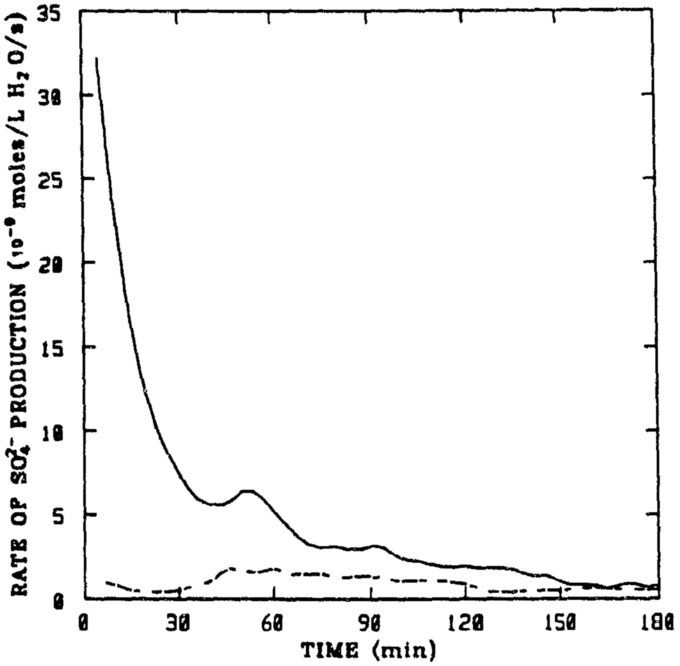

Figure 2.7 (a) Total rate of sulphate production per volume of cloud water by H_2O_2 (solid line) and O_3 (dashed line), vs time.

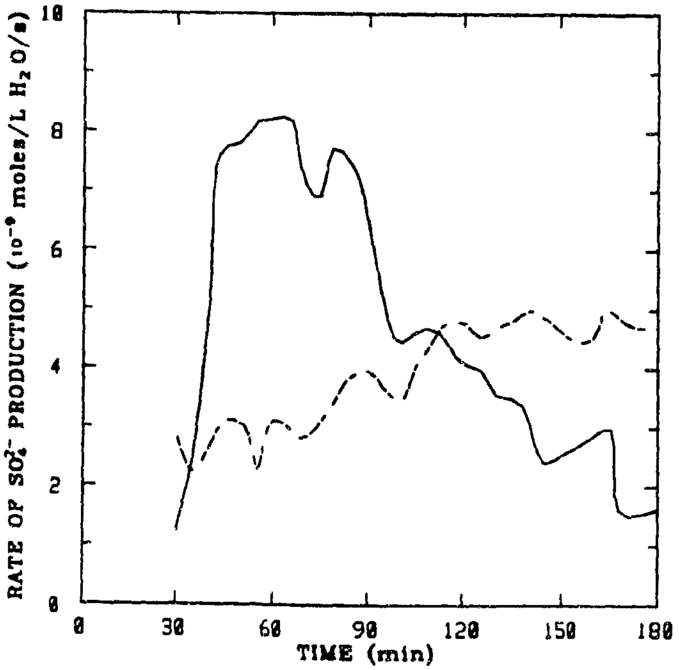

Figure 2.7 (b) Same as 2.7a but for rain.

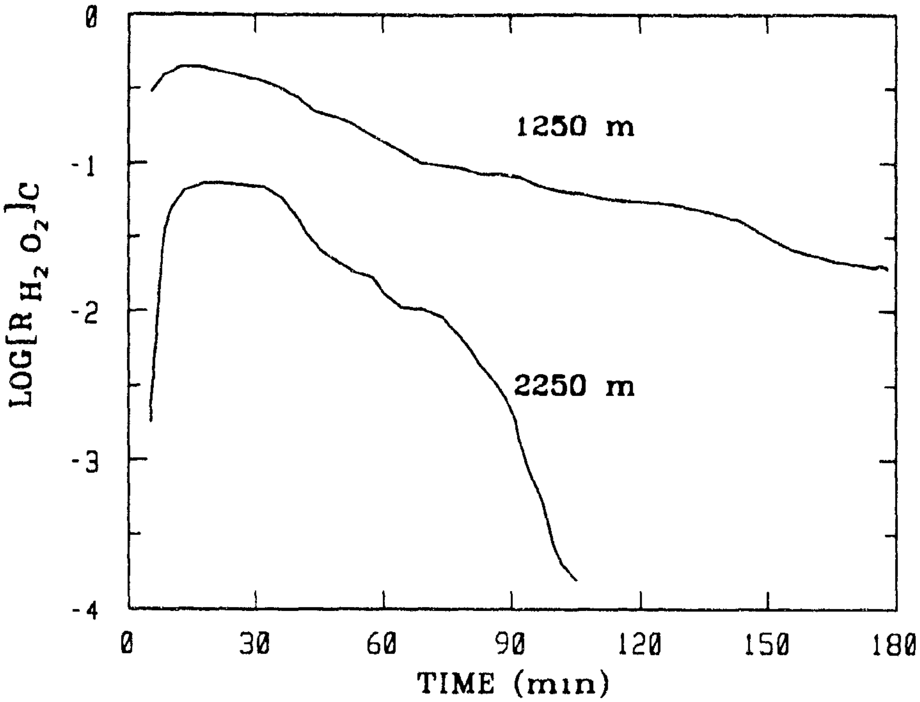

Figure 2.8 (a) Total rate of in-cloud oxidation (moles/s) of S(IV) by H_2O_2 at cloud base (1250 m) and 1 km above cloud base (2250 m).

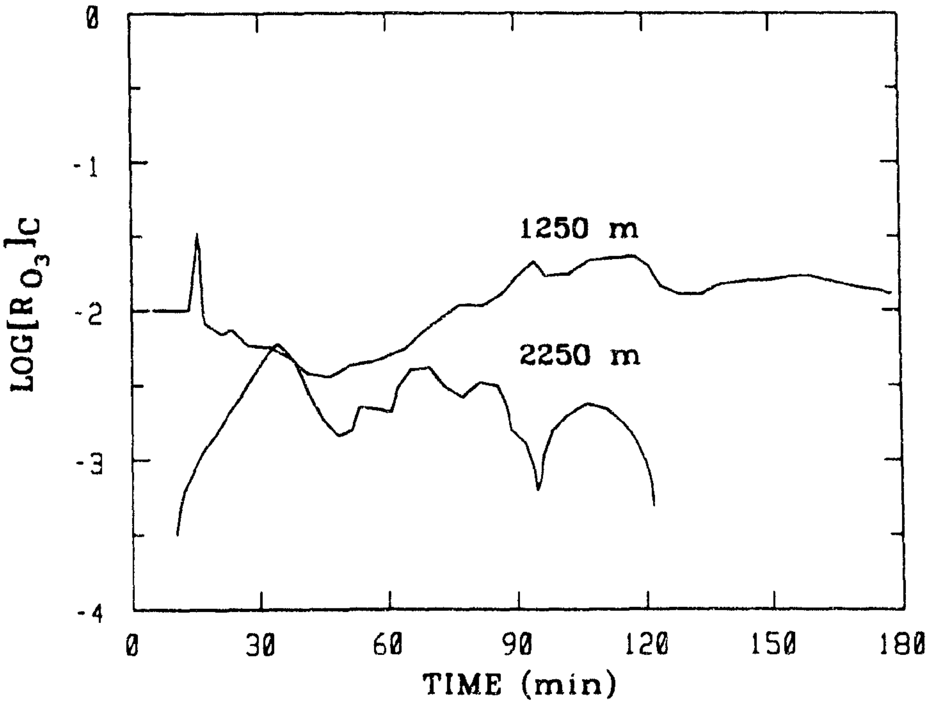

Figure 2.8 (b) Same as 2.8a but oxidation by O_3 .

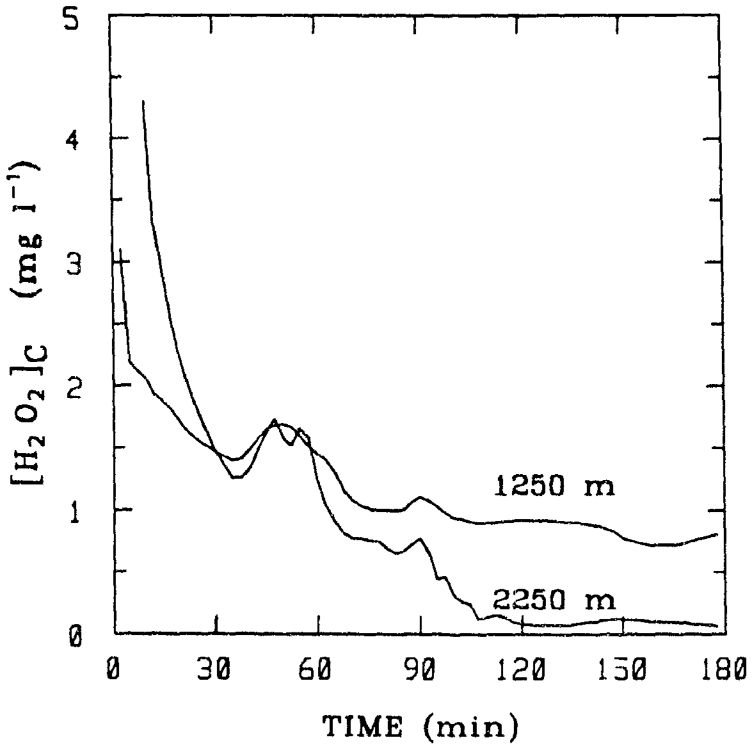

Figure 2.9 Average concentration of H_2O_2 (mg/L) dissolved in cloud at 1250 m and 2250 m, vs time.

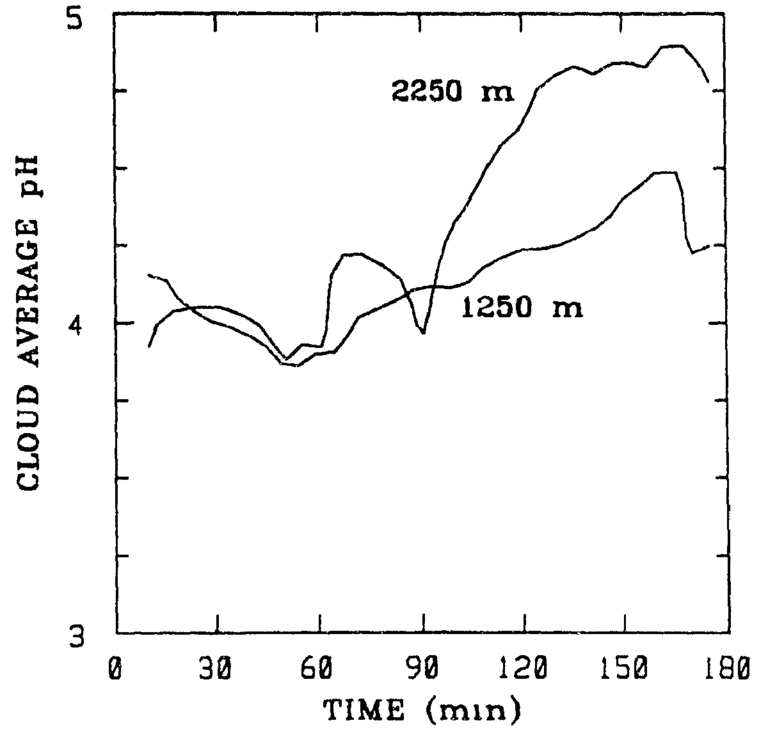

Figure 2.10 Average pH in cloud at levels 1250 m and 2250 m, vs time.

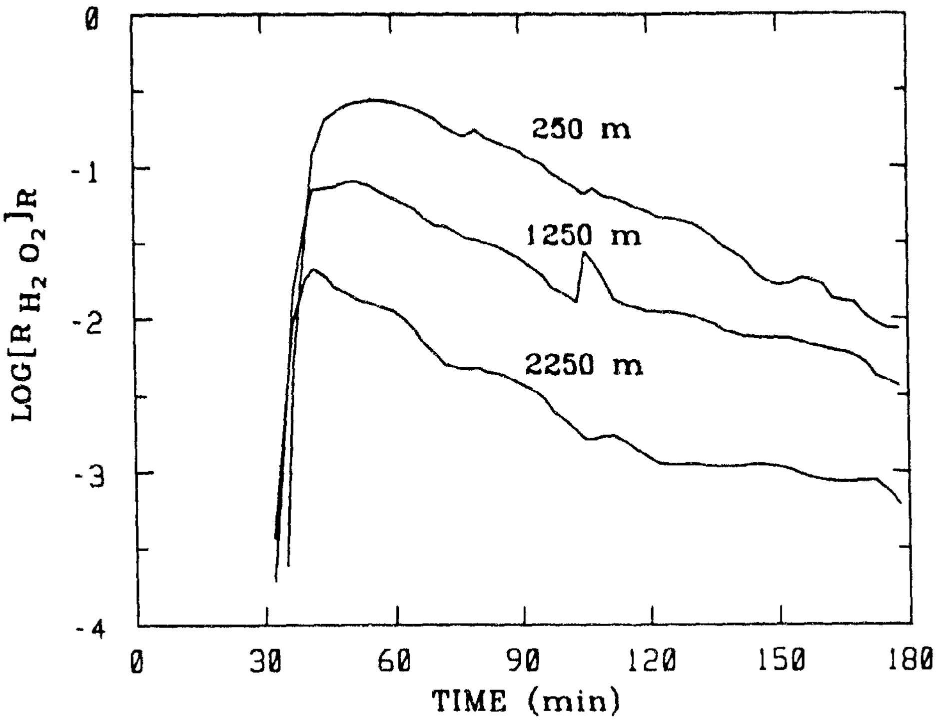

Figure 2.11 **(a)** Total in-rain oxidation rate of S(IV) by H_2O_2 (moles/s) at 2250 m, 1250 m, and 1 km below cloud base at 250 m.

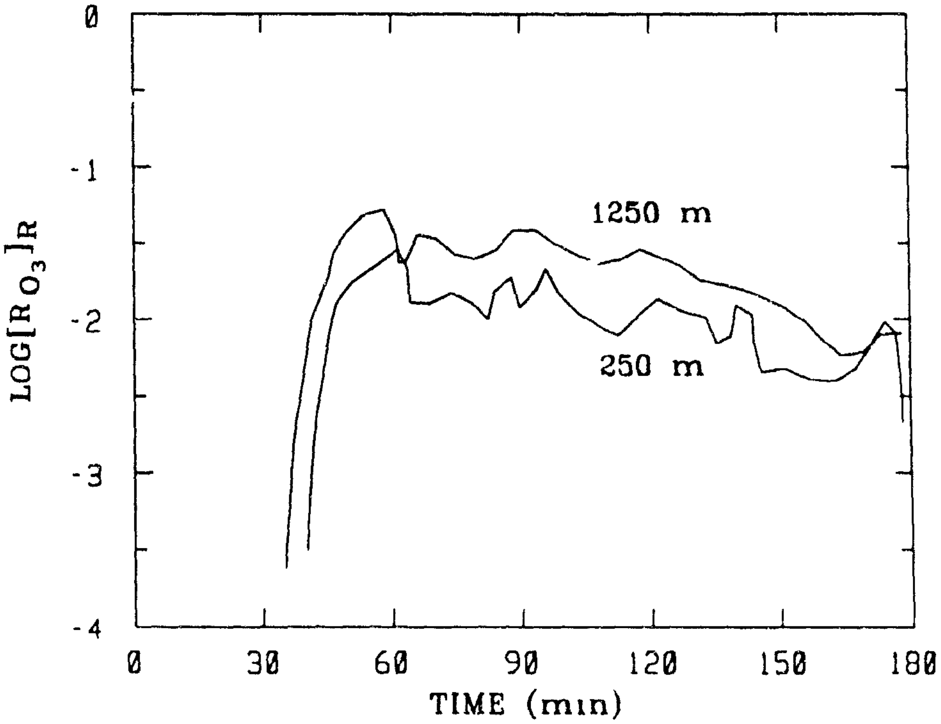

Figure 2.11 **(b)** Same as 2.11a but oxidation by O_3 at 1250 m and 250 m.

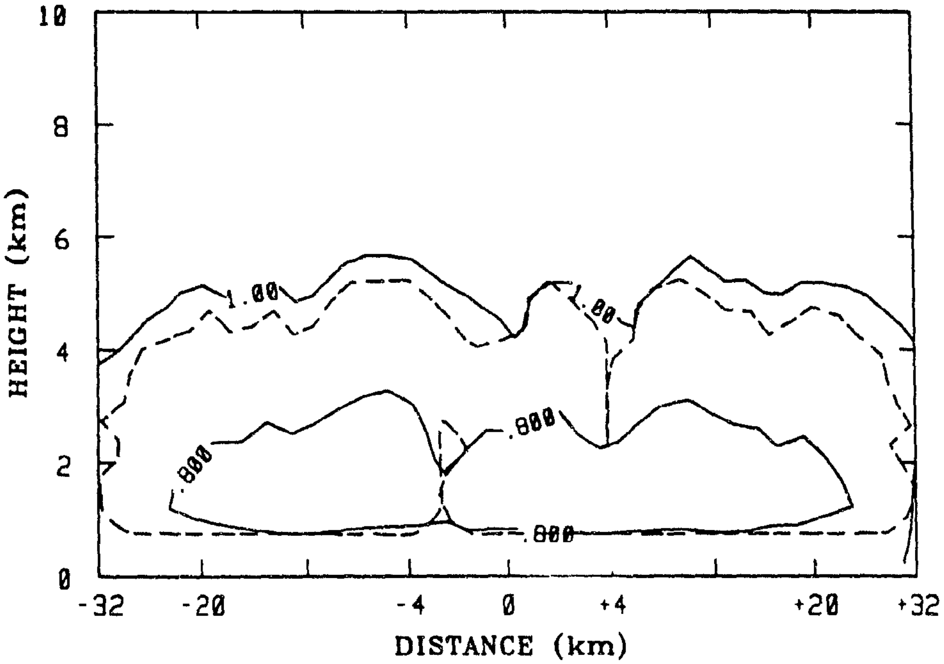

Figure 2.12 (a) Cross-section of concentration of H_2O_2 in air, cloud, and rain expressed in equivalent gas-phase units (ppbv) at 30 min. simulation time.

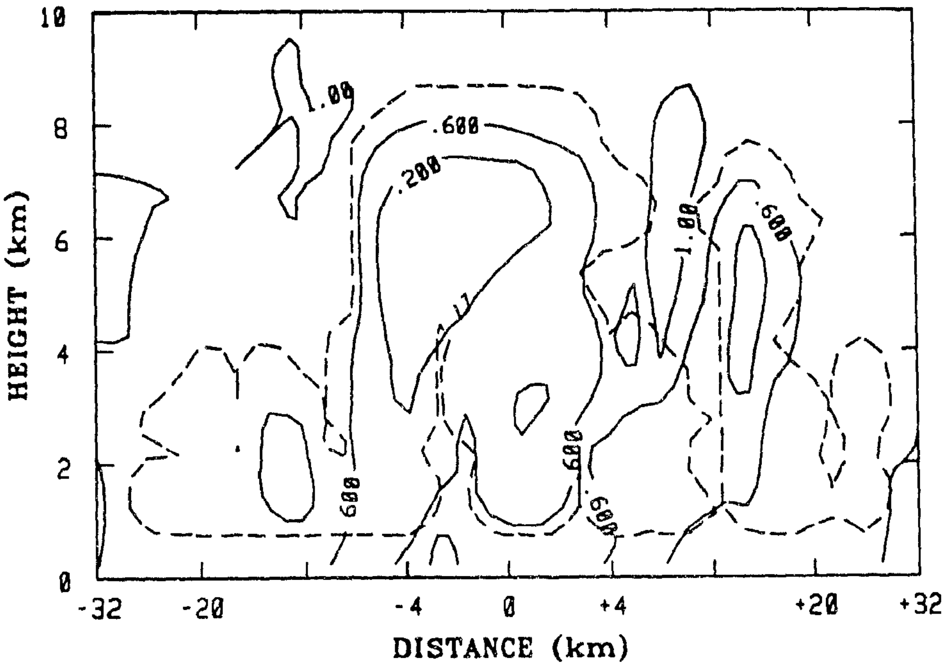

Figure 2.12 (b) Same as 2.12a but at 60 min.

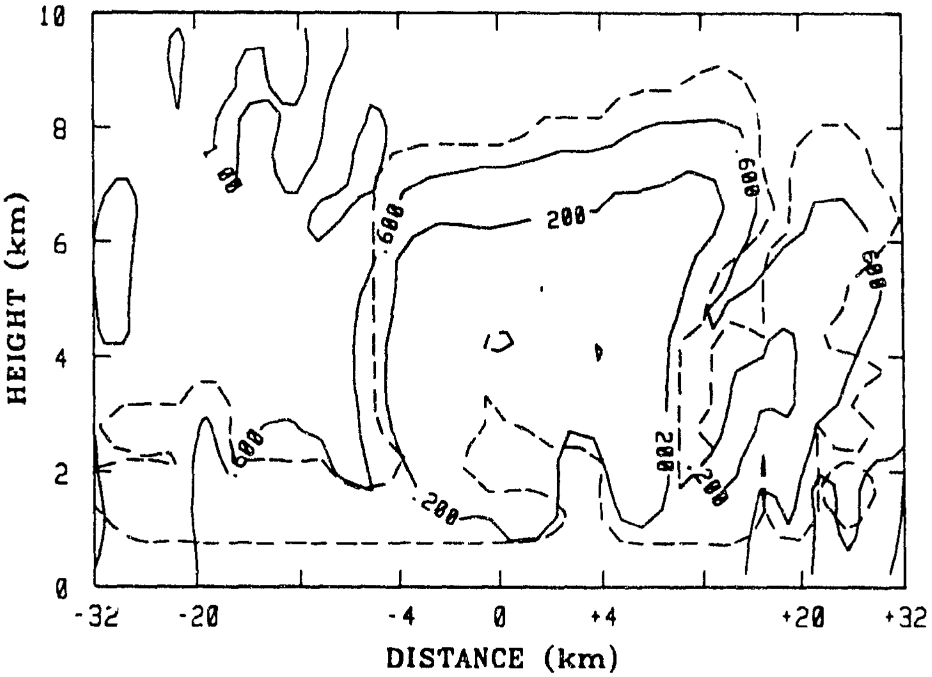

Figure 2.12 (c) Same as 2.12a but at 90 min.

CHAPTER 3

IN-CLOUD H_2O_2 PRODUCTION

3.1 Introduction

In the base simulation, aqueous-phase H_2O_2 was assumed to have come from the dissolution of $H_2O_{2(g)}$ from the cloud interstitial air. The results showed the initial dominance of H_2O_2 as oxidant and then its rapid depletion resulting in a reduction in the overall oxidation rate. Evidence has shown that the scavenging of hydroperoxy radicals by cloud droplets and subsequent reaction could be an additional source of hydrogen peroxide to cloud (Chameides and Davis, 1982; Schwartz, 1984b; McElroy, 1986).

In this chapter, the production of hydrogen peroxide in the aqueous phase by the disproportionation of two hydroperoxy radicals will be considered. The primary source of these radicals is through the scavenging of radicals from the gas phase. In order to determine the importance of this additional source of peroxide to the oxidation of SO_2 in a rainband, there are several processes that must be considered: (1) the gas-phase production and destruction rates of HO_2 radicals; (2) the rate of transfer of radicals from the gas-phase into cloud droplets; (3) aqueous-phase reactions of HO_2 radicals that result in peroxide production.

3.2 Mass transfer

To describe the transfer of HO_2 from the gas phase to the aqueous phase (as of any gaseous species) requires knowledge of its diffusion coefficients, its Henry's law solubility, and its accommodation coefficient for interfacial mass transport. The transfer of HO_2 from the gas phase into cloud droplets may be treated in one of two ways. In the limit of solubility equilibrium, the aqueous-phase concentration may be determined by Henry's law as discussed in Chapter 2. When the thermodynamic equilibrium is not attained, transfer must be treated explicitly by scavenging theory (Chameides and Davis, 1982; Hough, 1987). For the HO_2 radical, the second approach is necessary because these radicals are rapidly destroyed in the aqueous phase and therefore cannot reach sufficient concentrations to establish an equilibrium (Chameides, 1984).

The rate of mass transport may be written in reference to the gas- or aqueous-phase concentrations (Schwartz, 1984b):

$$\frac{d[n(HO_2)]}{dt} = -N_{drop}\,\phi_r\,(HO_2) \qquad \text{gas phase} \qquad (3.1)$$

$$\frac{d[HO_2]}{dt} = S_r^{\pm}(HO_2) \qquad \text{aqueous phase} \qquad (3.2)$$

where:

$n(HO_2)$ = gas-phase concentration of HO_2 (molecules/cm^3)
$[HO_2]$ = aqueous-phase concentration in moles/litre
N_{drop} = number of drops (cm^{-3})

$$S_r^{\pm}(HO_2) = \text{source of radicals to cloud}$$
$$= \phi_r(HO_2)/[\,4/3\pi r^3\ 6.02\text{x}10^{23}\,] \qquad (3.3)$$

$\phi_r(HO_2)$ = rate of transfer into and out of a single cloud drop of radius r (molecules/s)

$$= \frac{4}{3}\pi l r \left\{\frac{8R^* T}{m(HO_2)\pi}\right\}^{1/2} \left(1 + \frac{4l}{3r\alpha}\right)^{-1} \left\{ n(HO_2) - \frac{[HO_2]_T}{H_{eff} RT} \right\} \quad (3.4)$$

where α is the mass accommodation coefficient, l is the mean free path length, R^* is the gas constant (in J mol^{-1} K^{-1}), $m(HO_2)$ is the molecular mass of HO_2, and r is the radius of the drop. It should be noted in Equation 3.4 that at thermodynamic equilibrium there is no net transfer across the gas-liquid interface and the relation reduces to Henry's law:

$$n(HO_2) = \frac{[HO_2]_T}{H_{eff} RT} \quad (3.5)$$

The accommodation coefficient, defined as the fraction of collisions that result in a gas-phase molecule entering the aqueous phase, is a key parameter for describing the rate of interfacial transport. The frequency of radical scavenging is negligible for $\alpha<10^{-4}$ and increases approximately linearly with α for a value of α between 10^{-4} and 10^{-2}. For $\alpha \geq 10^{-2}$, the scavenging frequency becomes independent of α (Chameides and Davis, 1982). Mozurkewich et al. (1987) have measured the accommodation coefficient for HO_2 impinging on liquid water drops and have obtained a value of 0.2 s^{-1}. Schwartz (1984b) has shown that no interfacial mass transport limitation exists when $\alpha \geq 10^{-2}$. He has determined that there also is no mass transport limitation imposed by the aqueous- or gas-phase diffusion rates when pH≤5 and the partial pressure of HO_2 is approximately 10^{-12} atmospheres.

It has been suggested that the limiting step in the aqueous-phase disproportionation is the production of HO_2 in the gas phase (Chameides, 1984; McElroy, 1986). Instead of the gas phase (Chameides, 1984; McElroy, 1986). Instead of being controlled by thermodynamics, the concentrations of radicals in the two phases are controlled by a photochemical steady state in which the production of HO_2 is in balance with the loss of HO_2 by gas-phase reaction and loss of HO_2 to cloud drops (Chameides and Davis, 1982). This hypothesis will be used in this study to estimate H_2O_2 aqueous-phase production rates.

3.3 Gas-phase production and destruction rates of HO_2

Production and destruction rates of HO_2 in the troposphere may be estimated through the use of a simple gas-phase model. A set of reactions is used, adequate to describe the steady state concentrations of free radicals in the troposphere but simple enough to incorporate into the rainband chemistry model. The generation of OH radicals in the troposphere is mainly by the photolysis of O_3 to form $O(^1D)$ followed by the reaction of $O(^1D)$ with water.

$$O_3 + h\nu \xrightarrow{J_1} O(^1D) + O_2 \qquad \textbf{RG3.1}$$

$$O(^1D) + M \xrightarrow{k_{G2}} O(^3P) + M \qquad \textbf{RG3.2}$$

$$O(^1D) + H_2O \xrightarrow{k_{G3}} 2OH \qquad \textbf{RG3.3}$$

From these reactions, the steady-state $O(^1D)$ concentration may be written as:

$$O(^1D) = \frac{J_1 (O_3)}{k_{G2}[M] + k_{G3}[H_2O]} \qquad \textbf{(3.6)}$$

The concentration of HO_2 may be calculated by considering the dominant terms for the total sources and sinks of HO_x (H, OH, HO_2).

$$2k_{G3}\ O(^1D)\ (H_2O) = 2k_{G4}\ (OH)\ (HO_2)$$

where k_{G4} is the rate constant for RG3.4, the net loss of OH and HO_2.

$$HO_2 + OH \xrightarrow{k_{G4}} H_2O + O_2 \qquad \textbf{RG3.4}$$

And the instantaneous HO_2 concentration is:

$$HO_2 = \left[\frac{k_{G3}\ R_1}{k_{G4}} \quad O(^1D)\ (H_2O) \right]^{1/2} \tag{3.7}$$

where R_1 is defined as the ratio of HO_2 to OH radicals.

By assuming photochemical equilibrium for HO_2 and OH radicals in clear air and through the use of RG3.5 - RG3.8, R_1 may be approximated as:

$$R_1 = \frac{HO_2}{OH} = \frac{k_{G5}(O_3) + k_{G6}(CO)}{k_{G7}(O_3) + k_{G8}(NO)} \tag{3.8}$$

$$OH + O_3 \xrightarrow{k_{G5}} HO_2 + O_2 \qquad \text{RG3.5}$$

$$OH + CO \xrightarrow[O_2]{k_{G6}} CO_2 + HO_2 \qquad \text{RG3.6}$$

$$HO_2 + O_3 \xrightarrow{k_{G7}} OH + 2O_2 \qquad \text{RG3.7}$$

$$HO_2 + NO \xrightarrow{k_{G8}} OH + NO_2 \qquad \text{RG3.8}$$

For chosen concentrations of O_3=50ppb, NO=0.1ppb, CO=200ppb and reaction rate constants from Table 3.1, the value of R_1 is approximately 50.

In the presence of cloud drops, an additional loss term for HO_2 must be considered:

$$HO_{2(g)} \xrightarrow{k_9} HO_{2(aq)} \qquad \text{RG3.9}$$

where:

$$k_9 = N_{drop}\ \phi_r(HO_2)$$

The production of HO_2, loss in gas phase, and loss to cloud are then:

$$\left[k_{G5}(O_3) + k_{G6}(CO)\right](OH)=\left[k_{G7}(O_3) + k_{G8}(NO) + k_9\right](HO_2) \quad \textbf{(3.9)}$$

and by using the same method as for the clear air calculation, the concentration of HO_2 can be written as:

$$HO_2 = \frac{-R_1'k_9 + [\,(R_1'k_9)^2 + 4(2k_{G4})(2k_{G3}R_1'O(^1D)(H_2O))\,]^{1/2}}{2\,(2k_{G4})} \quad \textbf{(3.10)}$$

where R_1' is the ratio of HO_2 to OH derived from Equation 3.9.

To calculate the $O(^1D)$ concentrations via Equation 3.10, it is important to know the values of J_1 (the photolysis rate constant for ozone). The photolysis rates of ozone and thus the concentrations of $O(^1D)$ vary with the actinic flux or radiation available for reaction. Therefore it is necessary to determine how actinic fluxes vary within the rainband.

Table 3.1 Gas-phase reactions (Hough, 1987)

Reaction		Rate constants
RG3.1	$O_3 + h\nu \rightarrow O(^1D) + O$	J_1 (varies with flux)
RG3.2	$O(^1D) + M \rightarrow O(^3P) + M$	$k_{G2} = 2.1\text{x}10^{-11}\exp(100/T)$
RG3.3	$O(^1D) + H_2O \rightarrow 2OH$	$k_{G3} = 2.2\text{x}10^{-10}$
RG3.4	$OH + HO_2 \rightarrow H_2O + O_2$	$k_{G4} = 1.0\text{x}10^{-10}$
RG3.5	$OH + O_3 \rightarrow HO_2$	$k_{G5} = 1.9\text{x}10^{-12}\exp(-1000/T)$
RG3.6	$OH + CO \xrightarrow{O_2} CO_2 + HO_2$	$k_{G6} = 2.2\text{x}10^{-13}$
RG3.7	$HO_2 + O_3 \rightarrow OH + 2O_2$	$k_{G7} = 1.4\text{x}10^{-14}\exp(-600/T)$
RG3.8	$HO_2 + NO \rightarrow OH + NO_2$	$k_{G8} = 3.7\text{x}10^{-12}\exp(240/T)$
Units are:	s^{-1}	unimolecular
	cm^3 molecule^{-1} s^{-1}	bimolecular
	cm^6 molecule^{-2} s^{-1}	termolecular

3.4 Actinic fluxes and ozone photolysis rates

3.4.1 Photolysis rate coefficients

The photodissociation rate of a molecule A is defined by:

$$\frac{dn(A)}{dt} = - J(A)\ n(A) \qquad (3.11)$$

where n(A) is the concentration of A (cm^{-3}) and J(A) is the photolysis rate coefficient expressed in s^{-1} (Brasseur and Solomon, 1984). The photolysis rate of a species A is a function of its molecular absorption cross-section, the quantum yield or probability that molecule A decomposes on absorbing radiation of a certain wavelength, and the actinic flux available to the species. For example, the rate constant for RG3.1 may be expressed as:

$$J_1 = \int_{\lambda=295}^{320\ nm} F(\lambda,\theta)\ \sigma_{O_3}(\lambda)\ \phi_{O_3}(\lambda)\ d\lambda \qquad (3.12)$$

where J_1 = photolysis rate constant (s^{-1})
$F(\lambda,\theta)$ = actinic flux (photons / cm^2 / nm / s)
$\sigma_{O_3}(\lambda)$ = absorption cross-section (cm^2 / molecule)
$\phi_{O_3}(\lambda)$ = quantum yield

Reaction RG3.1 occurs between 295 and 320 nm. Sunlight shorter than 295 nm is mostly absorbed by stratospheric ozone, and at wavelengths longer than 320 nm the quantum yield of ozone approaches zero (Dickerson et al., 1979).

3.4.2 Definition of actinic flux

The actinic flux is defined as the flux on a spherical surface or the radiation intensity seen by a sample of absorbing species and integrated over all angles (Demerjian et al., 1980). It must be distinguished from the irradiance or horizontal flux which is the energy flowing through a horizontal surface. Both quantities may be calculated by integrating the radiance over all angles (Madronich, 1987):

Horizontal flux

$$E = \int_{\phi} \int_{\theta} L(\theta,\phi) \cos\theta \sin\theta \, d\theta \, d\phi \tag{3.13}$$

Actinic flux

$$F = \int_{\phi} \int_{\theta} L(\theta,\phi) \sin\theta \, d\theta \, d\phi$$

If the radiation intensity is isotropic, the actinic flux, F, equals $4\pi L$ where L is the radiance.

3.4.3 Model for δ-Eddington approximation

To determine the importance of free radical reactions, it is necessary to determine the effect of clouds on photolysis rates. Several approaches have been used to parameterize the effect of clouds. Chameides and Davis (1982) calculated cloud-free photolysis rates and then reduced these by a transmissivity factor to obtain in-cloud rates. Other investigators have used the two-stream method to approximate the actinic fluxes and thus the photolysis rates. The approach used here is as in Madronich (1987) and uses the delta-Eddington approximation to the radiative transfer equation (Joseph et al., 1976).

The delta-Eddington approximation calculates monochromatic fluxes directly in an absorbing-scattering atmosphere. It is an extension of the Eddington approximation to be applied to sharply forward-peaked phase functions. The phase function is approximated by a Dirac delta function forward-scattered peak and a two-term expansion for the remainder of the phase function. The phase function is written as:

$$P(\cos\theta) = 2f\delta(1 - \cos\theta) + (1 - f)(1 + 3g\cos\theta)$$

where f is the fraction of the scattered radiation in the forward peak and g is the asymmetry factor. The δ-Eddington approximation is equivalent to the Eddington approximation with layer optical parameters scaled as follows (Wiscombe, 1977):

$g^{'} = g / (1 + g)$	asymmetry factor
$\tau^{'} = (1 - \omega f)\tau$	optical depth
$\omega^{'} = (1 - f)\omega / (1 - \omega f)$	single-scatter albedo

Leighton (1980) incorporated the δ-Eddington approximation for a vertically inhomogeneous atmosphere (Wiscombe, 1977) into a model to compute heating rates in the atmosphere. This model was modified to calculate actinic fluxes for the wavelength band 295-320 nm.

The atmosphere is divided into 16 layers of varying thickness. The effective optical parameters for each layer are calculated as follows:

$$\tau = \sum \tau_i = \tau_R + \tau_{O_3} + \tau_M$$
$$\omega = \sum \tau_{sc,i} / \tau$$
$$g = \sum \tau_{sc,i}\, g_i / \tau_{sc}$$

where $\tau_{sc,i} = \omega_i \tau_i$, $\tau_{sc} = \Sigma\, \tau_{sc,i}$, and the subscript i labels the atmospheric component (τ_R is the Rayleigh optical thickness; τ_{O_3} is the optical thickness due to ozone; τ_M is the Mie optical thickness).

The model includes Rayleigh scatter, ozone absorption, and absorption and scattering by cloud droplets.

(a) Ozone absorption

Absorption by ozone is treated as in Fiocco (1978) (see Table 3.2) who uses a probability distribution for the absorption coefficients over a spectral interval $\delta\lambda$. For a particular layer, the absorption due to ozone would be:

$$A_{\delta\lambda}(u) = 1 - \sum_{i=1}^{M} a_i \, e^{-K_i u/\mu} \tag{3.14}$$

where a_i is the fraction of the interval $\delta\lambda$ occupied by the band with absorption coefficient near K_i. The vertical distribution of ozone is from the U.S. Standard Atmosphere with a total ozone column of 0.345 cm.

Table 3.2 Coefficients a_i, absorption coefficients K_i, and fraction of F_0 in the wavelength interval $\delta\lambda$.

$\delta\lambda$, A^0	a_i	K_i (cm^{-1})	fraction of F_0
2941 - 2985	0.127	21.5	1.98×10^{-3}
	0.593	17.8	
	0.278	13.6	
2985 - 3030	0.406	11.2	1.57×10^{-3}
	0.346	9.02	
	0.245	7.27	
3030 - 3077	0.116	6.50	2.08×10^{-3}
	0.603	5.43	
	0.278	4.16	
3077 - 3125	0.348	3.49	2.26×10^{-3}
	0.415	2.76	
	0.236	2.14	
3125 - 3175	0.261	1.84	2.59×10^{-3}
	0.463	1.48	
	0.275	1.14	

(b) Rayleigh scattering

Rayleigh scattering must be considered at short wavelengths. Coefficients for Rayleigh scatter are derived from values given by Penndorf (1957) (see Table 3.3). The Rayleigh volume scattering coefficient, β_R is a function of wavelength and also density of the layer.

Table 3.3 Rayleigh volume scattering coefficients at t=273 K, p=1013.25 mb. (from Penndorf, 1957)

Wavelength (nm)	β_R (km^{-1})
290	0.1765
300	0.1525
310	0.1325
320	0.1158

(c) Extinction by cloud

Vertical water profiles were those generated by the rainband model at several representative times during the simulation. The actinic fluxes and photolysis rates were calculated for three different microphysical cloud models with optical parameters taken from Stephens (1979). In the wavelength range, the single-scatter albedo is close to unity.

Table 3.4 Droplet distribution parameters (Stephens, 1979)

Cloud	Number of drops per cm^3	Liquid water content (g/m^3)	Mode radius (μm)
A	150	0.47	7.5
B	72	2.50	5.5,6.5
C	300	1.00	5.5

Table 3.5 Single scattering properties of chosen cloud microphysical models (values from Stephens, 1979)

Cloud	λ(nm)	σ_{ext} (km^{-1})	σ_{sca} (km^{-1})	$\tilde{\omega}_0$	$\langle \cos\theta \rangle$
A	0.30 0.33	73.46 73.03	73.46 73.03	0.999996 0.999997	0.866 0.863
B	0.30 0.33	120.03 120.23	120.03 120.23	0.999991 0.999994	0.862 0.862
C	0.30 0.33	126.68 126.67	126.67 126.67	0.999996 0.999997	0.860 0.856

3.4.3 Results

To maximize the potential effect of the HO_2 production, a solar zenith angle of 20^0 was chosen which corresponds to a midday value in southern Ontario in early July. Although the observed rainband occurred in November, there were no dynamics simulation input parameters that were season dependent. Because the dynamic fields were well simulated, they are being used as a laboratory, and a departure from comparison with observations must now be made.

To be consistent with the drop size assumed for the transfer processes, optical parameters for a stratocumulus cloud (Cloud A) were chosen (Stephens, 1979). Sensitivity tests were carried out using two other cloud types (Cloud B, Cloud C). Droplet distribution parameters and the single scattering properties are given in Tables 3.4 and 3.5.

Calculations were performed for cloud liquid profiles representative of various times in the rainband (30, 60, and 90 min). Several vertical profiles were chosen at each time and the average of these was the profile used. These liquid water profiles are shown in Figures 3.1a, b, c. At 30 minutes, the vertical extent of the cloud is less than that at 60 or 90 minutes but the liquid water content is greater.

Results of the delta-Eddington calculations of the O_3 photolysis rates in the rainband are shown in Figures 3.2-3.4. In the top layers of the cloud there is an enhancement in the ozone photolysis rate which is attributable to the effect of scattering of radiation by cloud droplets. Lower in the rainband, rates become less than those in clear air as the radiation is attenuated.

There is little difference between Clouds A and C while there is a slightly different profile for Cloud B. The maximum enhancement occurs for the profile at 30 minutes when the cloud liquid water content is highest. The maximum photolysis rate is below cloud top (4 km) with a value of approximately $6.4\text{x}10^{-5}$ s^{-1}. This rate is approximately 2.5

times the clear-air photolysis rate.

For the profiles typical of the rainband at 60 and 90 minutes, the rate maxima are within the cloud for Cloud B (6 km). The maxima for Clouds A and C are above cloud (8 km) with the rate dropping off more intensely below 6 km. For clouds at 60 and 90 minutes, the maximum rate is approximately $5.5\text{x}10^{-5}$ s^{-1} (2 times the clear air value).

Midway through the rainband, the rates become less than the clear air rates and below cloud base, rates are an order of magnitude less than those in clear air.

Although the optical parameters and liquid water profiles differ, there are features of the photolysis rate profiles common to all of the calculations: (1) Effect of scattering of radiation at cloud top enhances ozone photolysis rates; (2) Enhancement could be 2.5 times clear-air photolysis rates; (3) Below cloud base, photolysis rates are an order of magnitude less than those in clear air.

For the calculation of gaseous HO_2 concentrations, photolysis rates based on these profiles are used. Because the vertical rate decrease in the rainband is approximately linear, it is assumed that the radiation varies as follows:

$$J_1 = \frac{J_{TOP}(Z - Z_B) + J_{BASE}(Z_T - Z)}{Z_T - Z_B}$$

where

J_{TOP} = photolysis rate constant at cloud top (Z_T)
= $5.5\text{x}10^{-5}$ s^{-1}

J_{BASE} = photolysis rate constant at cloud base (Z_B)
= $2.0\text{x}10^{-6}$ s^{-1}

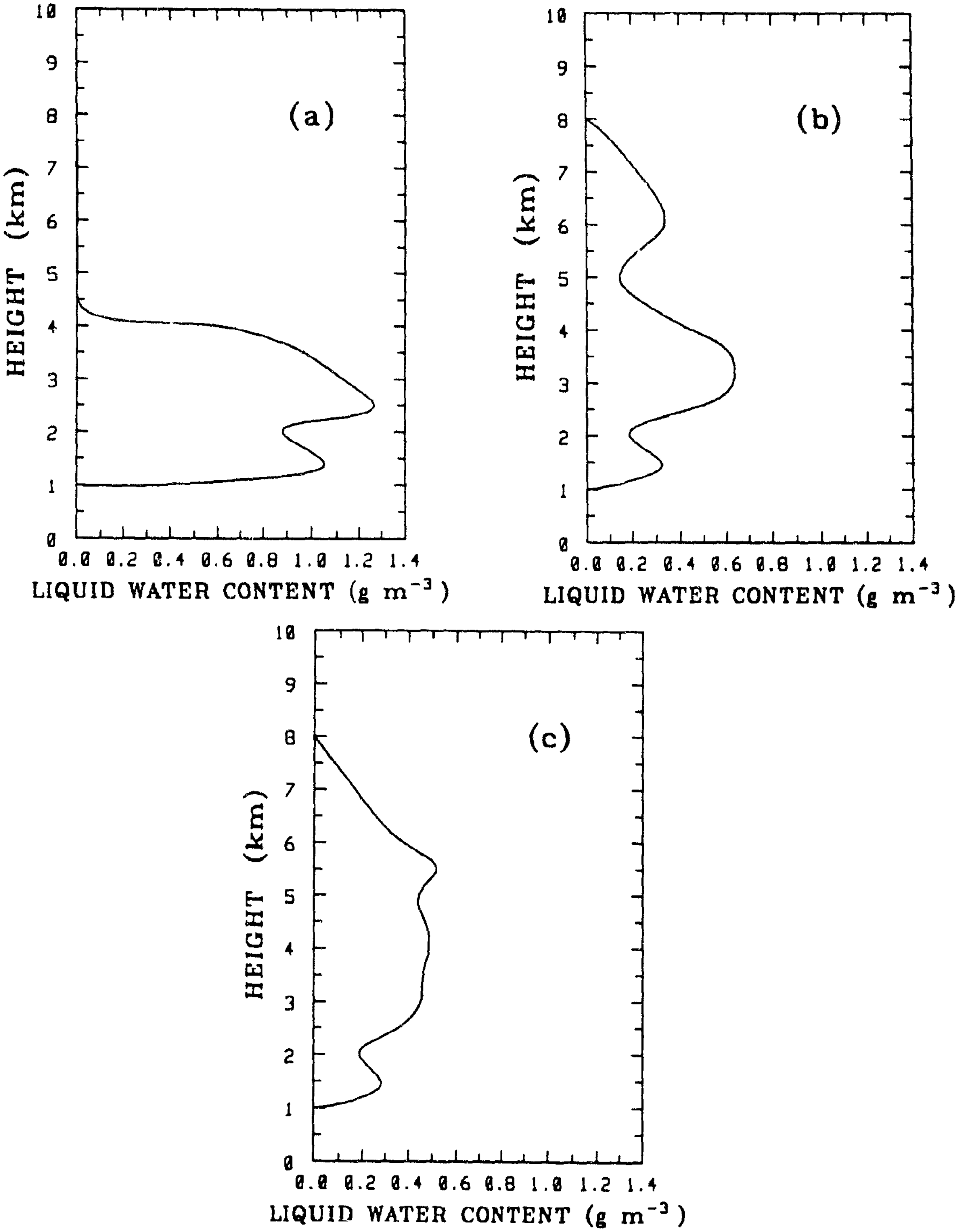

Figure 3.1 **(a)** Liquid water profile for cloud used in delta-Eddington calculation. Representative of rainband at 30 min.

(b) Same as 3.1a but for 60 min.

(c) Same as 3.1a but for 90 min.

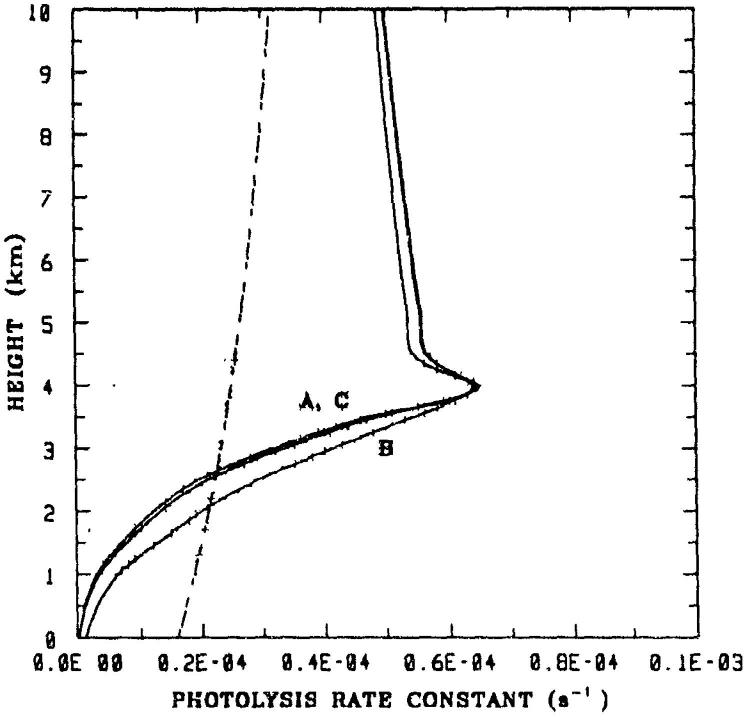

Figure 3.2 Ozone photolysis rates as a function of height in clear air (dashed line), and in the rainband at 30 min. Curves are identified for Clouds A, B, and C.

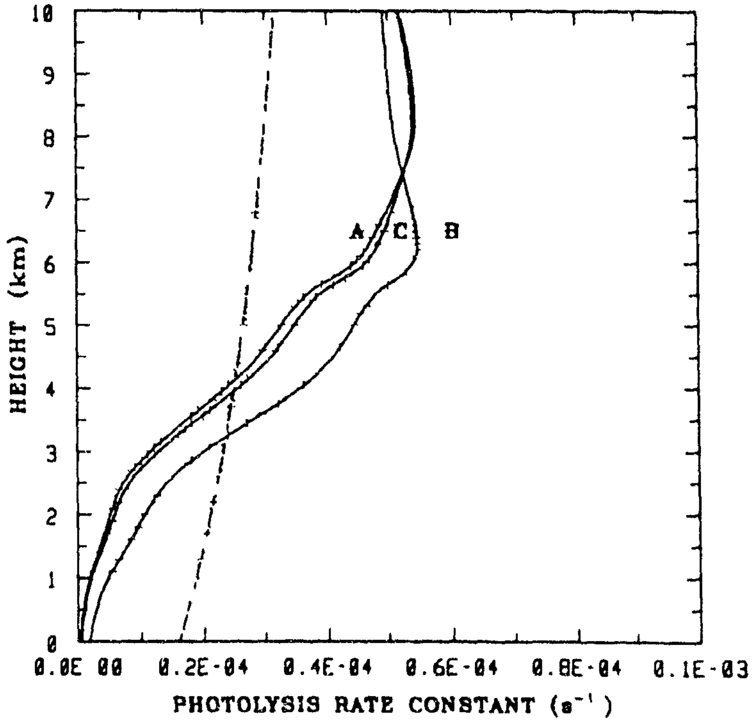

Figure 3.3 Same as 3.2 but for 60 min.

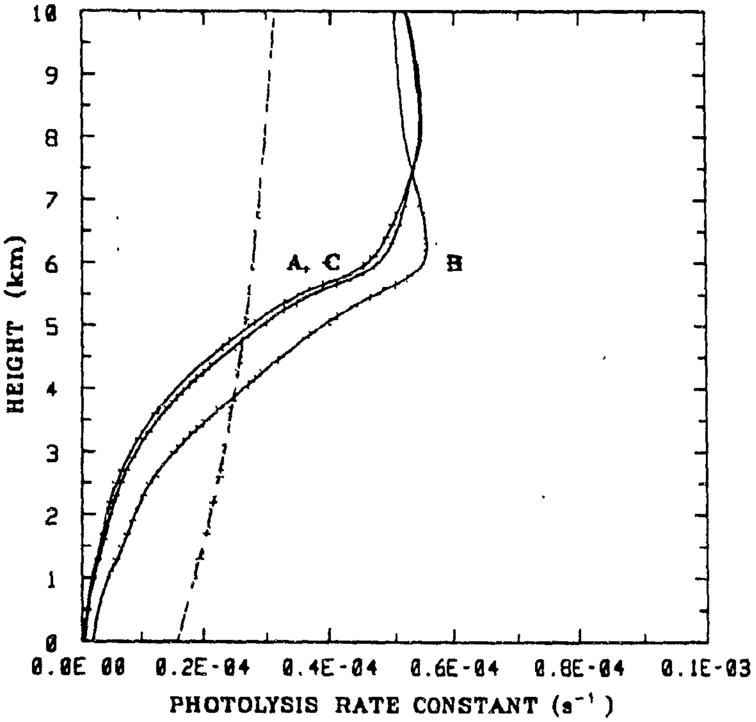

Figure 3.4 Same as 3.2 but for 90 min.

3.5 Aqueous-phase reactions

The HO_2 radical dissociates in cloud to form O_2^- and H^+.

$$HO_2 \leftarrow\rightarrow O_2^- + H^+ \qquad \textbf{RA3.1}$$

The equilibrium constant, K_{eq}, can then be written as:

$$K_{eq} = \frac{[O_2^-]\,[H^+]}{[HO_2]}$$

and the total reactant species in rapid equilibrium can then be considered as a single entity (Schwartz, 1984b):

$$HO_{2_T} = HO_2\left[\,1 + K_{eq}/\,[H^+]\,\right] \qquad \textbf{(3.15)}$$

Disproportionation of HO_2 to form H_2O_2 occurs via three different routes:

$$HO_2 + HO_2 \xrightarrow{k_{A2}} H_2O_2 + O_2 \qquad \textbf{RA3.2}$$

$$HO_2 + O_2^- \xrightarrow[H^+]{k_{A3}} H_2O_2 + O_2 \qquad \textbf{RA3.3}$$

$$O_2^- + O_2^- \xrightarrow[H_2O]{k_{A4}} HO_2^- + O_2^- + OH \qquad \textbf{RA3.4}$$

Reaction RA3.4 is relatively unimportant as a production pathway for H_2O_2 therefore it is not necessary to include it (McElroy, 1986). The total rate of H_2O_2 production (Reactions RA3.2, RA3.3) may be written as:

$$\frac{d[H_2O_2]}{dt} = k_{A2}[HO_2]^2 + k_{A3}[O_2^-]\,[HO_2] \qquad \textbf{(3.16)}$$

or in terms of the total HO_2:

$$\frac{d[H_2O_2]}{dt} = k^* \ [HO_{2_T}]^2$$

where: (3.17)

$$k^* = \frac{k_{A2} + k_{A3}K_{eq}/[H^+]}{\left(1 + K_{eq}/[H^+]\right)^2}$$

In addition to the formation of H_2O_2, HO_2 in its dissociated form O_2^-, reacts with ozone in solution representing a competition for peroxide production.

$$O_2^- + O_3 \xrightarrow{k_{A5}} O_3^- + O_2 \qquad \text{RA3.5}$$

This sink is pH dependent and could be a significant loss of $HO_{2(aq)}$ at high pH (McElroy, 1986). If there were no competing reaction, we could expect one molecule of peroxide produced for every two HO_2 radicals scavenged. McElroy found that at a pH of 5 there was approximately one molecule of H_2O_2 formed for every four HO_2 radicals scavenged. Because the average pH values of cloud in the base simulation range from about 4.0-5.0 it is necessary to include the effect of the competing reaction.

Chameides (1984) calculated times for HO_2 radicals to establish a thermodynamic equilibrium across the gas-liquid interface. Because the aqueous-phase chemical lifetime of HO_2 radicals is short compared to the time needed to reach equilibrium, Chameides has suggested that the concentrations are controlled by the photochemical steady state (described in Section 3.3) rather than by thermodynamics. Based on this hypothesis, we assume that the amount of HO_2 reaction in cloud drops in one timestep is limited by that transferred from the gas phase. Therefore in one timestep, an upper limit of HO_2 reacting cannot exceed that transferred from the gas phase. Or in one timestep we can say:

$$S_r^+ = S_r^- [HO_{2_T}] + 2\,k^* [HO_{2_T}]^2 + \frac{k_{A5}\,K_{eq}}{[H^+]\left(1 + K_{eq}/[H^+]\right)} [HO_{2_T}][O_3] \qquad (3.18)$$

where $S_r^{\pm}$ are as defined by Equation 3.3 and includes transport into and out of the cloud drops (S_r^+ is transport into drop, S_r^- is transport out of drop).

The resulting source of H_2O_2 to cloud is described by Equation 3.17 where HO_{2_T} is given as:

$$HO_{2_T} = \frac{-C_2 + (C_2^{\,2} + 4\,C_1\,S_r^+)^{1/2}}{2\,C_1}$$

where:

$$C_1 = \frac{2\left(k_{A2} + k_{A3}\,K_{eq}/[H^+]\right)}{\left(1 + K_{eq}/[H^+]\right)^2}$$

$$C_2 = S_r^- + \frac{k_{A5}\,[O_3]\,K_{eq}}{[H^+]\,(1 + K_{eq}/[H^+])}$$

Table 3.6 Aqueous-phase reactions (Pandis and Seinfeld, 1989); litre-mole units

Reaction	Rate/Equilibrium constant
$HO_{2(g)} \leftrightarrow HO_{2(aq)}$	$H_{HO_2} = 2.0\times10^{3}\exp(6640(X^{*}))$
RA3.1 $HO_{2(aq)} \leftrightarrow H^{+} + O_2^{-}$	$K_{eq} = 3.5\times10^{-5}$
RA3.2 $HO_{2(aq)} + HO_{2(aq)} \rightarrow H_2O_2 + O_2$	$k_{A2} = 8.6\times10^{+5}\exp(-2365(X))$
RA3.3 $HO_2 + O_2^{-} \xrightarrow{H_2O} H_2O_2 + O_2 + OH^{-}$	$k_{A3} = 1.0\times10^{+8}\exp(-1500(X))$
RA3.4 $O_2^{-} + O_2^{-} \xrightarrow{2H_2O} H_2O_2 + O_2 + 2OH^{-}$	$k_{A4} < 0.3$
RA3.5 $O_2^{-} + O_3 \xrightarrow{H_2O} OH + 2O_2 + OH$	$k_{A5} = 1.5\times10^{+9}\exp(-1500(X))$
	$^{*}X = (1/T - 1/298)$

CHAPTER 4

RESULTS OF SIMULATION WITH H_2O_2 PRODUCTION

4.1 Introduction

The numerical simulation to be discussed in this chapter will examine the effect of in-cloud hydrogen peroxide production on the sulphate formation in the rain-band. The same dynamic fields and initial chemical profiles that are employed in this simulation (Simulation 2) are those that were used in the base simulation. Through the use of the set of gas-phase reactions described in Section 3.3 and the use of the δ-Eddington approximation to calculate ozone photolysis rates, the gas-phase HO_2 concentrations were estimated. Radicals are scavenged by drops and react to produce H_2O_2. The objective of this simulation was to estimate an upper limit for peroxide production in cloud. It is for this reason that actinic fluxes and ozone photolysis rates are calculated with an input solar zenith angle of 20^o. And with the upper estimate of this additional source of aqueous-phase peroxide, the effect on sulphate production and sulphate deposited to the surface can be seen. Because the concentration of peroxide was initially high and peroxide was clearly the dominant oxidant early in the base simulation, any effect of additional H_2O_2 was not expected to be seen in the first 30 min. of the three hour run. It is in the later stages of the simulation, when H_2O_2 had been significantly depleted, that a positive effect might be expected.

4.2 Source of H_2O_2 to drops

As mentioned in Chapter 3, the ozone photolysis rates vary from a value of 2.0×10^{-6} s^{-1} at cloud base to 5.5×10^{-5} s^{-1} at the top of cloud. In clear air these photolysis rates, along with the chemical concentrations and reaction rates as discussed in Section 3.4 would lead to steady-state gaseous HO_2 concentrations of air of about 5 ppt to a maximum of 25 ppt. In the presence of cloud drops the additional loss mechanism, that of scavenging by the drops, can further reduce the gas phase HO_2 concentrations. Because a monodisperse cloud droplet distribution with a fixed radius has been assumed, an increase in cloud liquid water content means an increase in the number of drops available for scavenging. So in regions of high liquid water, a larger fraction of the $HO_{2(g)}$ is transferred to cloud. For example, for a liquid water content of 1 g/m^3, the $HO_{2(g)}$ concentrations can be reduced to about 1 ppt. The scavenging rate expression varies with the cloud drop radius - small drops being more efficient scavengers. In this study, the drop radius is 10 μm. For 10 μm drops and a liquid water content of 1 g/m^3, the value of k_9 (see Section 3.4), the fractional removal rate of HO_2 from the gas phase to the aqueous phase, is approximately 0.3 s^{-1}. The values of k_9 for drops of 5 - 20 μm range from about 1.3 to 0.09 s^{-1}.

Scavenging of HO_2 radicals by raindrops is not considered for two reasons: (1) The size of the raindrops is larger than cloud drops and the scavenging rate would therefore be slower; (2) Much of the rain is in the lower levels of the domain and below cloud base. In these regions, the concentrations of radicals is lower than higher in the domain and again scavenging would be unimportant.

Source strengths of the radicals to cloud drops were calculated as in Equation 3.3. The source strength for a photolysis rate of 5.5×10^{-5} and liquid water content of 1 g/m^3 is about 1.6×10^{-9} M s^{-1}. (This compares well with the source term calculated by Chameides and Davis (1982) of 7.3×10^{-10} M s^{-1} for a solar zenith angle of 30^0, liquid water content of 1.5 g/m^3 and approximately 100 $drops/cm^3$). The corresponding steady state HO_2 concentration is 2.7×10^6 $molecules/cm^3$. This source leads to an aqueous-phase production rate of H_2O_2 of 7.4×10^{-10} M s^{-1} at a pH of 4.0. The rate is reduced as the pH increases because of the competition from the reaction of ozone and the dissociated form of HO_2.

The strength of the competing reaction is a function of pH. Where the source strength of HO_2 radicals is low (of order 10^{-10} M s^{-1}), there are approximately 2.3 molecules of HO_2 scavenged to produce one molecule of H_2O_2 at pH 3. At a pH of 5, 7.2 radicals are scavenged for 1 molecule of H_2O_2. Where the source strength is high (1.6×10^{-9} M s^{-1}), the effect of the competing reaction is less dependent on pH. Numbers of radicals scavenged to produce one molecule of H_2O_2 range from 2.1 at a pH of 3 to 2.8 at a pH of 5. For the whole simulation, the ratio of HO_2 radicals scavenged to molecules of H_2O_2 formed is 3.7. This value agrees quite well with the one given by McElroy (1986) who suggests a yield of 1 H_2O_2 molecule for every 4 HO_2 radicals scavenged at a pH of 5.

4.3 Rates of H_2O_2 production

Perhaps the rates of peroxide production can be examined more clearly if they are expressed in units comparable to those describing the initial profile. Results of the calculations of H_2O_2 production rates are shown in Figures 4.1a-d for 30, 60, 90, and 120 minutes simulation time. The production rates are expressed in ppbv/h. Recall that the initial concentration of peroxide in the domain was uniform at 1 ppb. Typical production rates are 0.1 - 0.3

ppbv/h. As expected, rates are enhanced near cloud top - a typical value there being approximately 0.5 ppbv/h. At 30 min., the combination of high liquid water content and scattering of radiation causes a $H_2O_{2(aq)}$ production rate of 0.5 ppbv/h over a significant part of the rainband.

Enhanced rates can also be seen in the trailing edges of the rainband. Again, this can be attributed to the sum of elevated photolysis rates (approximately 5.0×10^{-5} s^{-1}) yet greater liquid water contents (approximately 0.5 g/m^3) than high in cloud (about 0.1 - 0.2 g/m^3 at 8 km). Although these rates (0.9 ppbv/h) are high, they are not over a large volume of the domain and therefore do not cause a large increase in the H_2O_2 generated. These rates are close to values calculated by Walcek (1988) of 0.5 ppb/h near cloud top although the zenith angle used for the calculations was not explicitely stated. For a zenith angle of 30^0, Chameides and Davis (1982) calculated production rates of 0.3 - 0.6 ppb/h varying as the number of drops per cubic centimeter varied.

It is useful to compare total H_2O_2 (air, cloud, rain) with H_2O_2 in the base run. Figures 4.2a - d show the difference in peroxide concentration between Simulation 2 and the base run every 30 min. from 30 to 120 min. At 30 min. (Fig. 4.2a), an increased concentration of 0.1 ppb can be seen throughout the whole cloud and an increase of 0.2 ppb in top levels where there is a higher production rate and less SO_2 for oxidation reaction. At 60 min. (Fig. 4.2b) and especially at 90 min. (Fig. 4.2c) it can be seen that the increase is less than 0.1 ppb in areas corresponding to the cloud updrafts. It is in these regions that much of the oxidation occurs and H_2O_2 produced in or transported to these regions is still lost to reaction. From these results, however, it seems that in certain areas of the domain, there could be elevated gas-phase levels of H_2O_2 upon evaporation of cloud.

4.4 Result of H_2O_2 source on sulphate production

The overall effect on sulphate produced during the simulation is illustrated in Figure 4.3. The total moles of sulphate formed in cloud and rain may be compared to those produced in the base simulation. It is not surprising that there is little difference early in the simulation when the concentration of peroxide was high. It is at approximately 25 minutes that the effect of the additional peroxide on the production of sulphate can be seen. Over the three hour period, there is a 10% increase in the number of moles of sulphate formed in cloud and a 23% increase in rain. The large relative increase in rain is not surprising because in the base simulation when rain formed the concentration of H_2O_2 had already been significantly diminished. Even though there is no H_2O_2 production in rain, the H_2O_2 produced in cloud equilibrates between air and cloud before it is lost to reaction with SO_2. Thus not only is there more H_2O_2 transferred from cloud to rain, there is also more transferred from air to rain.

Now that it is evident that there is an increase in the total H_2O_2 in the domain, the concentration of H_2O_2 dissolved in cloud could be examined level by level. In Chapter 2, concentration of H_2O_2 in cloud was plotted and its depletion could be seen as the simulation progressed. Figure 4.4a gives the concentration of H_2O_2 in cloud at 3250 m and 6250 m relative to that of the base simulation. At 3250 m, there is an initial increase in the peroxide concentration reaching a peak of 0.52 mg/L more at 60 min. but the addition lessens as more SO_2 is transported to this level reacting with H_2O_2. High in the cloud (6250 m), the concentration continues to increase throughout the simulation.

The corresponding differences in concentrations of sulphate in cloud are plotted in Figure 4.4b. At 3250 m, the sulphate change closely follows the peroxide change. At this level, an increase in peroxide effected an increase in sulphate. The result, however, is not the same at 6250 m. Although there is an increase in the peroxide dissolved in cloud, there is no equivalent increase in sulphate concentration. In fact the averaged SO_4^{2-} concentrations decrease slightly. Because more SO_2 now is being oxidized below 6250 m, less is being advected to that level. These figures indicate that at lower levels in the cloud, the production of sulphate is limited by the amount of oxidant available, but higher in the rainband SO_2 itself is the limiting factor.

The net change in H_2O_2 as a function of height is shown in Figure 4.5. It is the difference between the total peroxide produced and the total peroxide lost by oxidation of SO_2 in cloud and rain. In both simulations, the bulk of the oxidation occurs just above cloud base. Above approximately 2250 m, there is a net gain in peroxide but below 2250 m there is a net loss. In Simulation 2, there is more oxidation by H_2O_2 below cloud base. Although there is no peroxide produced at these levels, peroxide produced higher in the domain is carried by rain below cloud. The moles of peroxide transferred from air to rain and from cloud to rain increase by 20% and 31% respectively.

A brief comment is needed at this point on the effects of the diffusion scheme that is used in the model. It was noted in Chapter 2 that the model includes a rather unconventional formulation of diffusional effects. Instead of the chemicals diffusing to attain a vertical profile with zero gradient, they diffuse to restore their initial profiles. This scheme was introduced by Pitre (1986) to approximate an hypothesized large-scale forcing mechanism that was maintaining the clear air chemicals outside the band area. Without this type of diffusion the chemicals tended to diffuse rapidly upwards - something that was not observed in the field study. It is possible that because of this scheme, the effects of vertical advection of pollutants in updrafts are being diminished. In the case of pollutants being advected from low domain levels to high, this diffusion form will tend to have a stronger effect of returning chemicals to lower levels than a conventional scheme would. A sensitivity study was carried out by comparing the present results with results from a simulation that included a regular diffusion form. At the end of 90 minutes (recall that most of the oxidation has taken place by this time), there was a 10% increase in the overall oxidation. Because more SO_2 could be transported to upper levels, there was a shift spatially in where the oxidation occurred. There was more oxidation in cloud and less in rain below cloud base.

Finally if the bottom line in a study involving acid precipitation is the sulphate in rain and the sulphate deposited to the surface, a comparison of these quantities with the same from the base simulation is needed. This additional sulphate formed causes only a 6% increase in the amount of sulphate transferred from cloud to rain and a 3% increase in the amount of sulphate deposited on the ground. Obviously for this rainband, the increased sulphate production is insignificant in view of the importance of nucleation and scavenging of sulphate aerosol as a mechanism of incorporating sulphate. Although for this run it is inappropriate to compare sulphate concentrations in air and rain with observations from the Isaac et al. (1983) field study, it is nonetheless useful to make a comparison of values given in Table 2.3 with similar values in Simulation 2 (see Table 4.1). The only differences between the quantities in the two simulations are in the sulphur dioxide concentrations in air, indicating that more SO_2 is transferred to cloud and rain where it is oxidized but also indicating the overwhelming importance of sulphate aerosol in clear air for determining the sulphate deposited on the surface.

Table 4.1 Concentrations from Simulation 2 and measured concentrations of sulphur dioxide in air, sulphate in air, and sulphate in rain just above and below cloud base. Numbers in parenthesis below observed values are high and low values reported.

Time (min)	$[SO_2]_a$ (µg/kg)	$[SO_4^{=}]_a$ (µg/kg)	$[SO_4^{=}]_r$ (mg/L)
Observed (1250 m)	5.0 (1.6-11.4)	2.6 (0.7-5.6)	2.2
90 min	1.75	3.95	1.22
100	1.67	3.98	0.94
110	1.57	4.07	0.96
120	1.50	4.16	0.79
Observed (750 m)	7.3 (0.0-15.8)	4.0 (0.6-9.0)	1.8
90 min	3.82	6.63	1.61
100	3.73	6.65	1.13
110	3.63	6.68	1.31
120	3.53	6.70	1.07

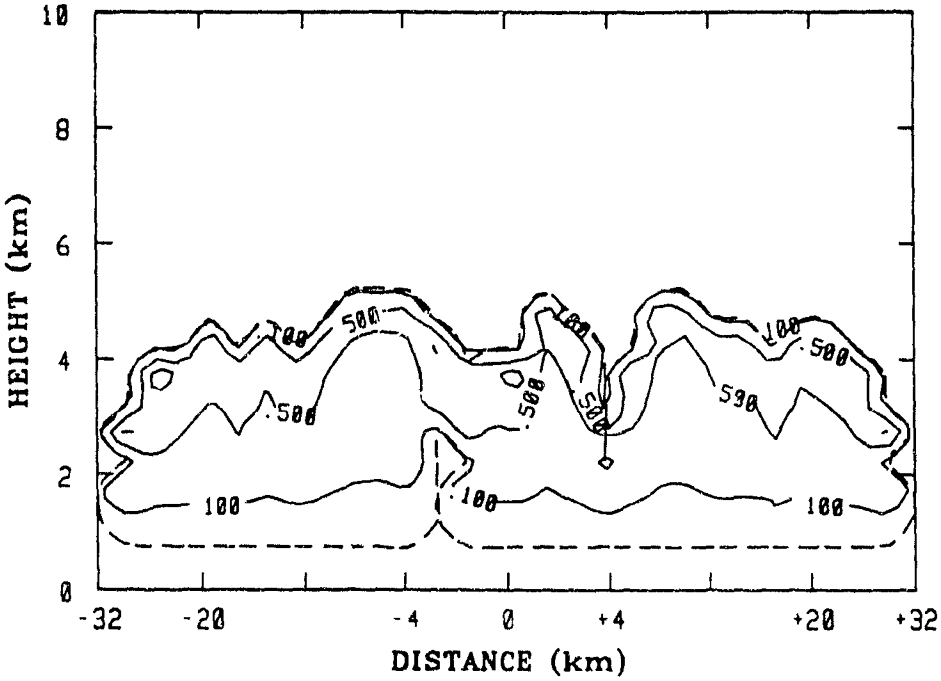

Figure 4.1 **(a)** Vertical cross-section of production rates (ppb/h) of H_2O_2 in cloud at 30 min.

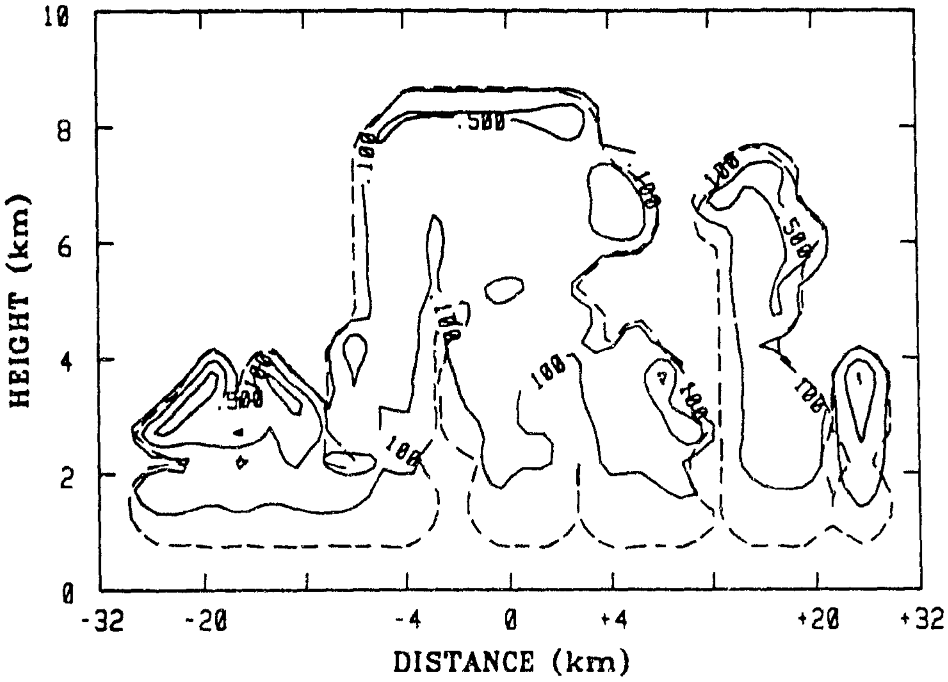

Figure 4.1 **(b)** As in 4.1a except at 60 min.

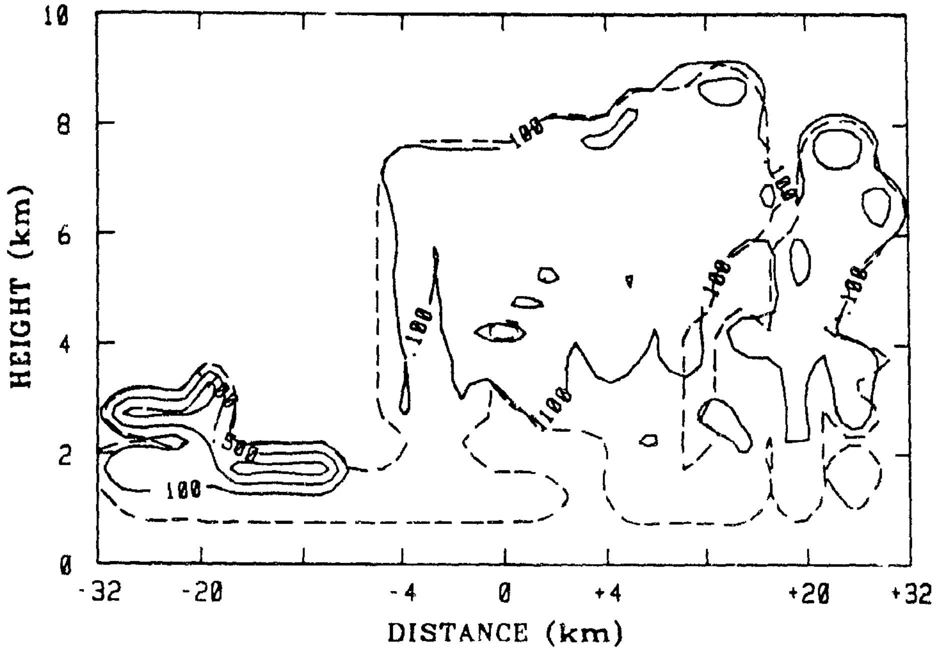

Figure 4.1 (c) As in 4.1a except at 90 min.

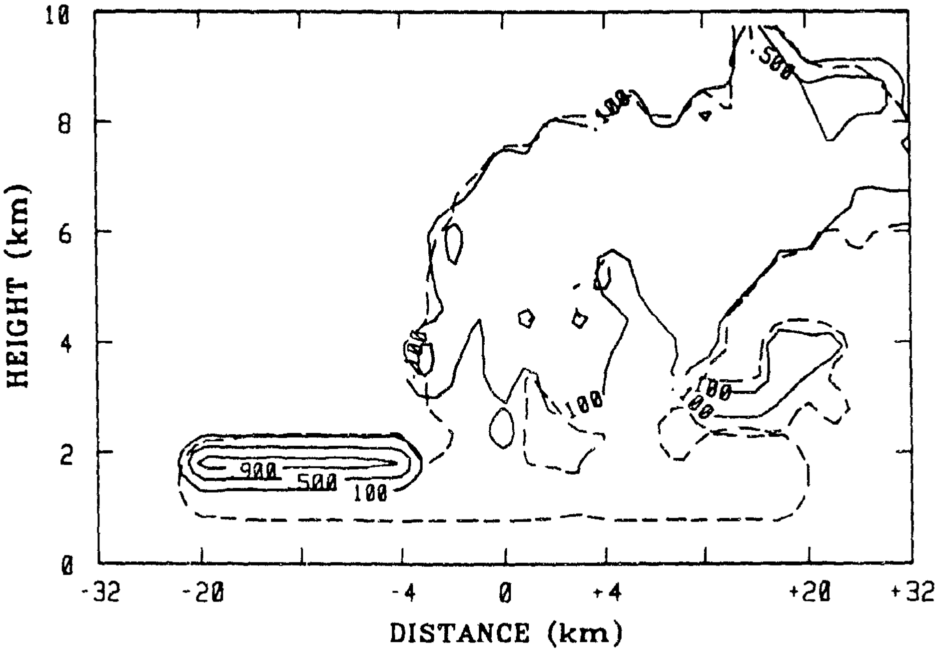

Figure 4.1 (d) As in 4.1a except at 120 min.

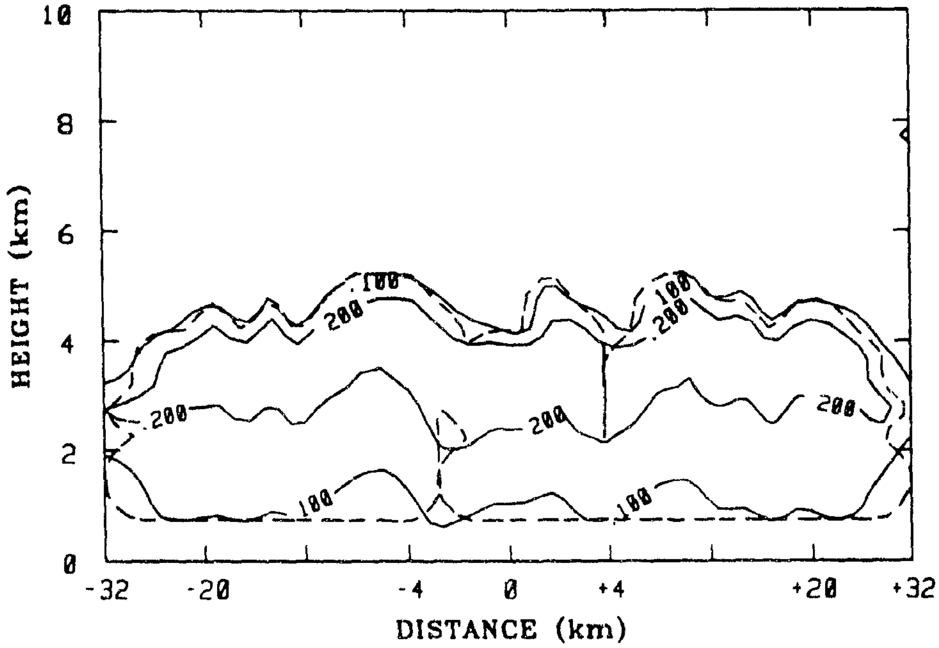

Figure 4.2 (a) Vertical cross-section of difference between total H_2O_2 (ppbv) in Simulation 2 and total H_2O_2 in the base simulation at 30 min.

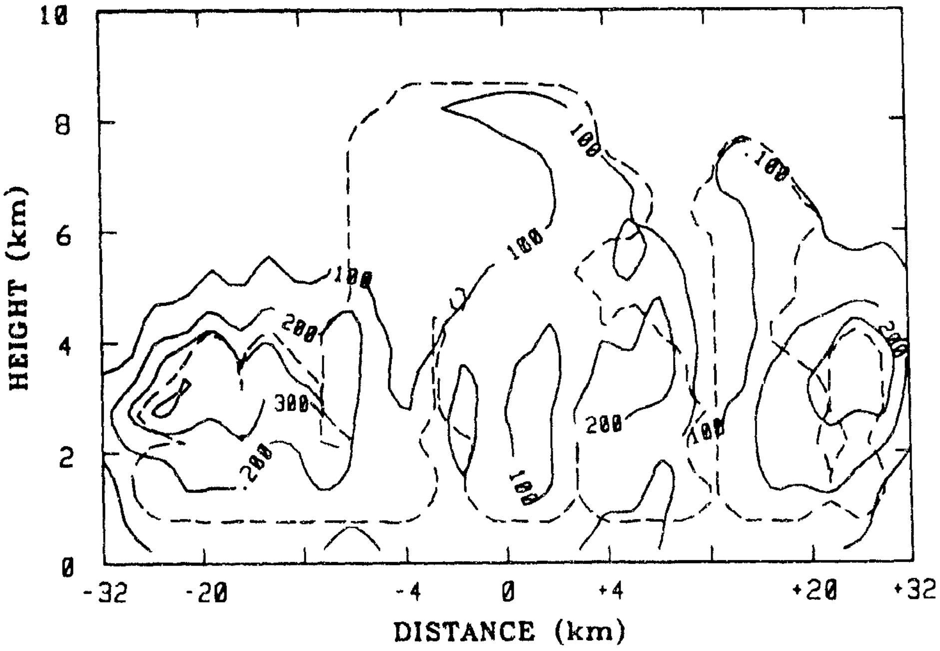

Figure 4.2 (b) As in 4.2a except at 60 min.

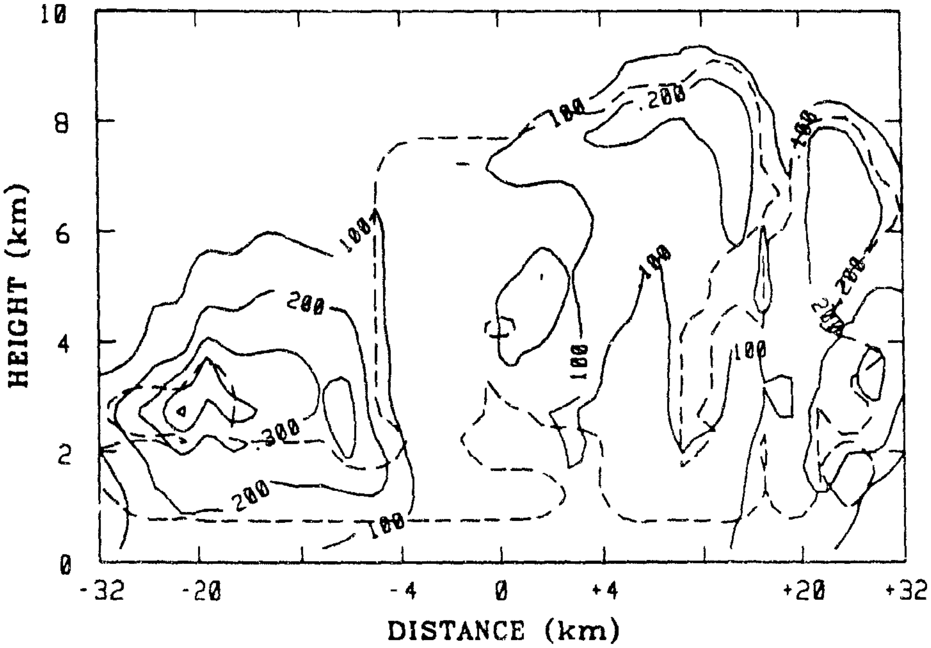

Figure 4.2 (c) As in 4.2a except at 90 min.

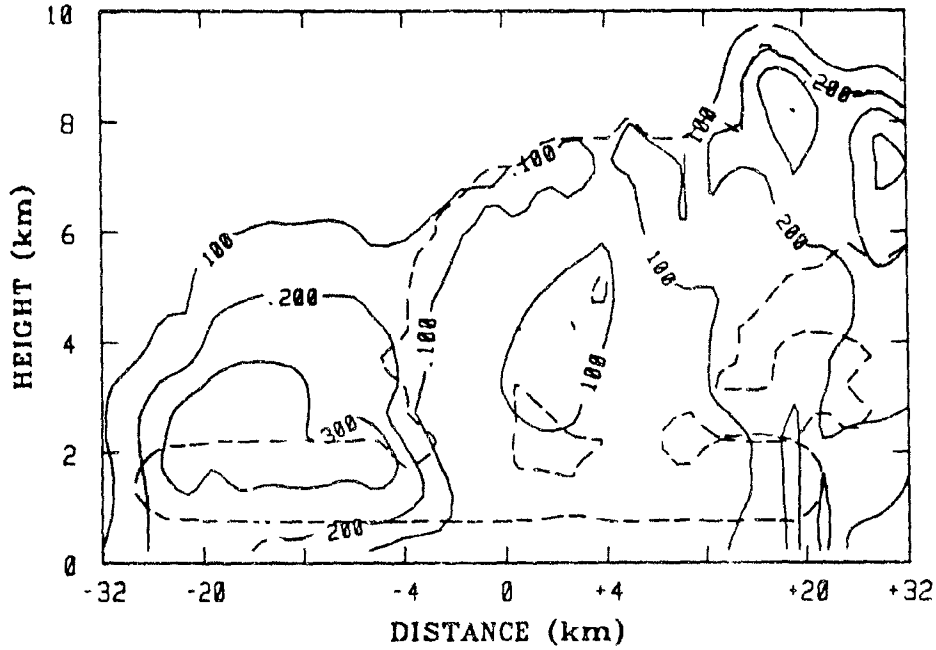

Figure 4.2 (d) As in 4.2a except at 120 min.

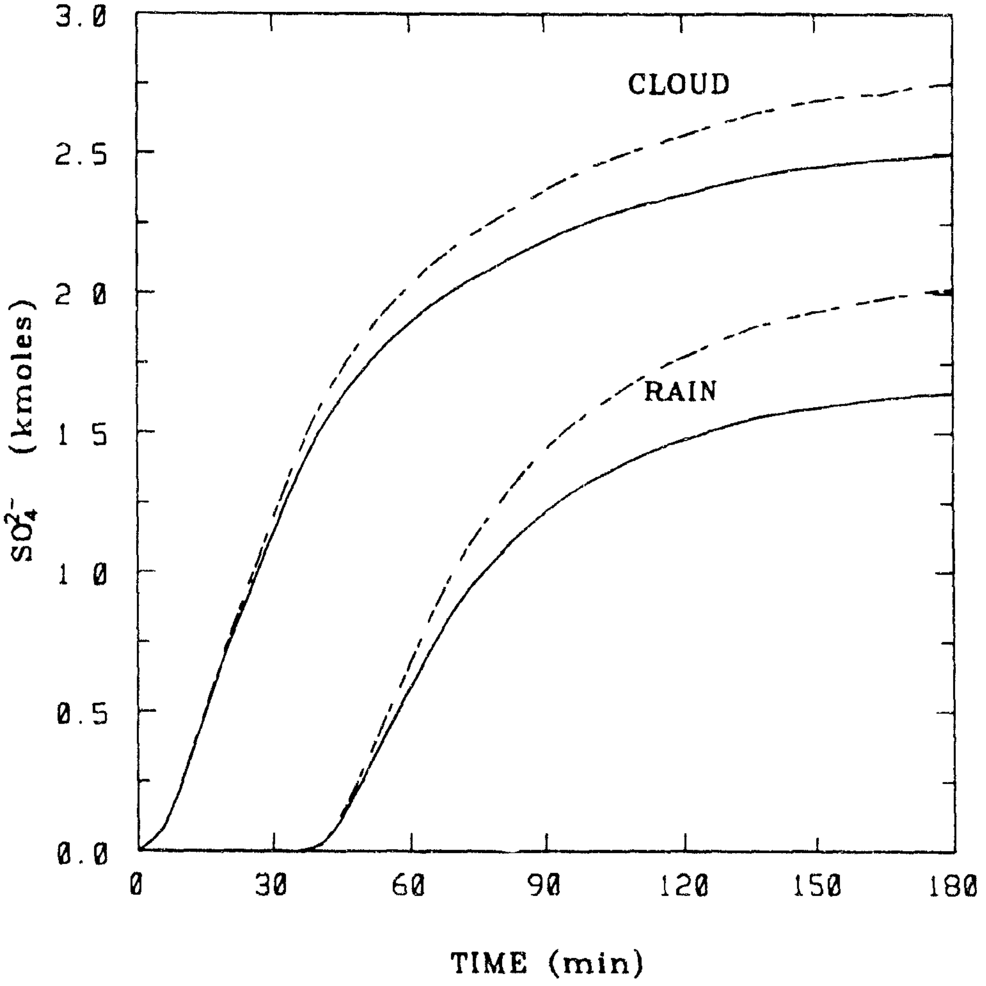

Figure 4.3 Total moles of sulphate formed in cloud and rain by H_2O_2 reaction in the base simulation (solid lines) and Simulation 2 (dashed lines).

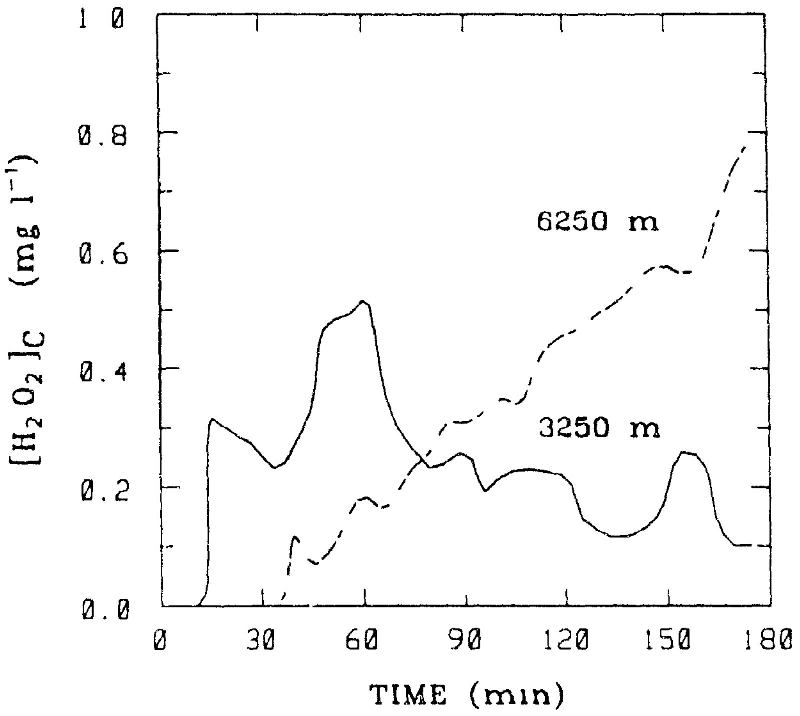

Figure 4.4 **(a)** Difference in the concentration of H_2O_2 in cloud (mg/L) between Simulation 2 and the base simulation at 3250 m and 6250 m, vs time.

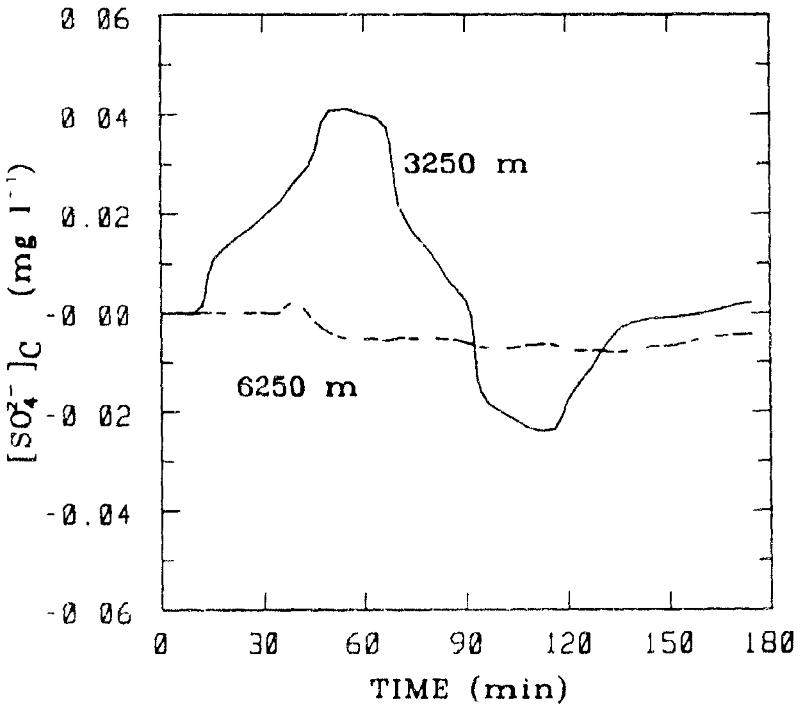

Figure 4.4 **(b)** As in 4.4a except for sulphate in cloud.

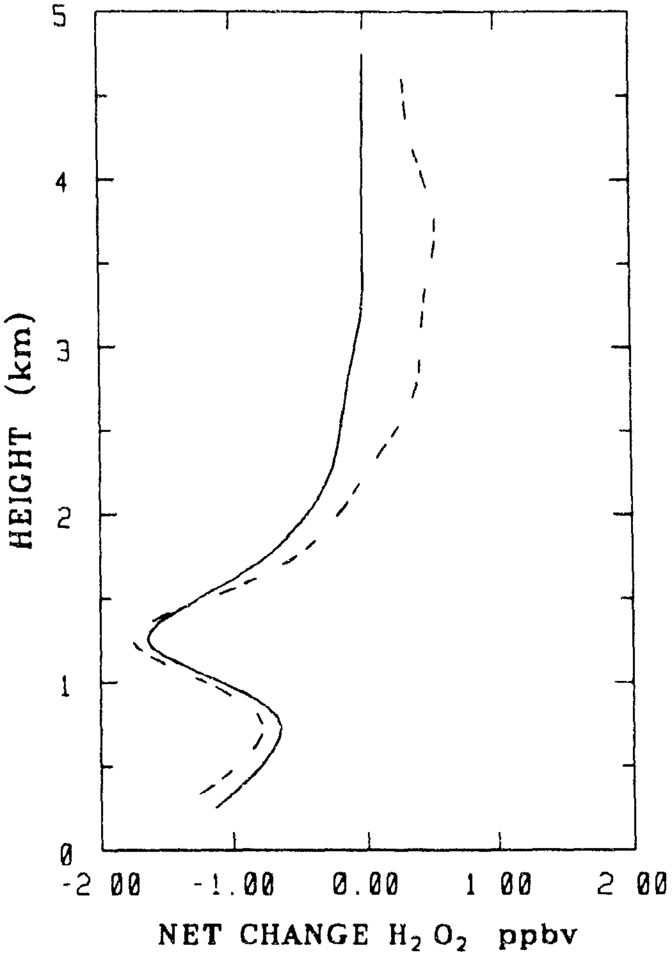

Figure 4.5 Net change in H_2O_2 (ppb) as a function of height in Simulation 2 (dashed line) and the base simulation (solid line).

CHAPTER 5

SUMMARY AND CONCLUSIONS

5.1 Introduction

As increasing numbers of detrimental effects of pollution are seen on terrestrial ecosystems, the need to understand formation, transport, and deposition of pollutants becomes more urgent. It is essential to know the relationship between emission of SO_2 and deposition of SO_4^{2-} if cost-effective emission control strategies are to be developed. In clouds, not only chemical but also microphysical and dynamical processes contribute to establishing this link. Gas-phase formation of sulphate is linear in SO_2 (Heikes et al., 1987). The extent to which sulphate formation in clouds is oxidant limited is uncertain but it is thought to be dependent on the concentrations of H_2O_2 and O_3 (Calvert et al., 1985).

There is an interest in H_2O_2 because of the nature of its reaction with SO_2. Unlike the reaction of O_3 and SO_2 which is highly pH dependent - decreasing with increasing pH, the reaction of H_2O_2 and SO_2 is approximately independent of pH. Therefore, provided that there are sufficient concentrations of H_2O_2, the reaction can still be important even at low pH. Hydrogen peroxide is produced in the gas phase but it has also been hypothesized that significant production from the scavenging and reaction of HO_2 radicals could take place within cloud.

In cloud chemistry models, gas-phase reactions are important for determining the profiles of chemicals in clear air when the cloud forms. Over the lifetime of a single cloud, the additional amount of pollutants produced in the gas phase is considered to be negligible. Therefore the majority of cloud chemistry models begin with gas-phase profiles and then consider only aqueous-phase reactions. In longer-lived mesoscale systems such as rainbands, the neglect of gas-phase processes may be a less valid assumption. One possible effect on the oxidation of SO_2 is the aqueous-phase production of H_2O_2 following gas-phase production of HO_2 radicals and transfer of radicals to cloud drops. In this thesis, a two-dimensional numerical model of cloud chemistry has been used to investigate the effect of this additional source of H_2O_2 on the oxidation of SO_2 in a rainband.

5.2 Overview

In Chapter 2, a description of the simulation which served as a base for comparison was described. The chemistry model required dynamic fields as input and the fields used are those simulated by Valton (1986) to describe a rainband which formed in southern Ontario on November 5, 1981. The base simulation included HNO_3, NH_3, SO_2, CO_2, H_2O_2, O_3 and a sulphate aerosol (mixture of H_2SO_4 and $(NH_4)_2SO_4$). Oxidation could occur via reaction with H_2O_2 or O_3. No in-cloud source of H_2O_2 was included; $H_2O_{2(aq)}$ came from the dissolution of $H_2O_{2(g)}$, present before the cloud formed.

Some of the results include a dominance of H_2O_2 as oxidant early in the simulation but a decrease in its contribution to sulphate formation was observed as its concentration became depleted. The relative contributions of H_2O_2 and O_3 to the oxidation of SO_2 differed from cloud to rain. H_2O_2 accounted for 84% and 62% of sulphate produced in cloud and rain respectively. The relatively substantial contribution of O_3 to the oxidation of SO_2 in rain as compared to cloud could be attributed to lower H_2O_2 concentrations and higher pH values which favour the O_3 reaction.

A large portion of the sulphate to enter cloud and rain came from the nucleation and scavenging of sulphate aerosol. This accounted for approximately 75% of the sulphate that entered both cloud and rain. The relative amount is high not only because the initial aerosol concentration in air is high but also because the overall oxidation rate dropped off as the simulation progressed. An additional source of peroxide to cloud could perhaps increase the sulphate production at later times during the simulation.

A method for examining the potential effects of in-cloud H_2O_2 production was then discussed in Chapter 3. It was assumed that the aqueous-phase reaction is limited by the rate of production of HO_2 radicals in the gas phase. The hypothesis of Chameides (1984), that the relative concentrations of HO_2 in the gas and aqueous phases are controlled by a photochemical steady state, has been used. In this steady state, the production of HO_2 is in balance with its loss in the gas phase and loss to cloud drops.

Because the production of HO_2 radicals is initiated by the photolysis of ozone, a major part of the estimation of production rates has been the calculation of ozone photolysis rates in the rainband. The δ-Eddington approximation to the radiative transfer equation was used and the variation of actinic flux and photolysis rates was determined. Calculations were made for liquid water profiles representative of different times during the simulation and for three different cloud microphysical models. Results showed an enhancement of photolysis rates at the top of the band with values of approximately 5.5×10^{-5} s^{-1}. Rates below the band were about an order of magnitude slower with a typical value of 2.0×10^{-6} s^{-1}.

Using the calculated photolysis rates, a simple set of gas-phase reactions, and interfacial transport as in

Chameides (1984), the source of HO_2 to cloud was estimated. Source terms varied as a function of liquid water content and the photolysis rate of ozone. The source terms were highest in the trailing edges of the rainband. In these regions liquid water contents of about 0.5 g/m^3 and high photolysis rates combined to give an enhanced source.

The source term was related to aqueous-phase H_2O_2 production by using the assumptions that H_2O_2 production is limited by the production of HO_2 in the gas phase. Therefore in one timestep the upper limit of the amount of HO_2 that reacts is that which can be transferred from the gas phase. If every HO_2 radical scavenged went on to produce H_2O_2, one would expect one molecule of H_2O_2 formed for every two HO_2 radicals scavenged. In this study, the reaction of O_3 with HO_2 in its dissociated form is included as a competing reaction. Over the whole simulation, there were approximately 3.7 radicals scavenged for each H_2O_2 produced. This value agrees quite well with the ratio of 4.2 at a pH of 5.0 calculated by McElroy (1986).

The in-cloud production rates of H_2O_2 varied in the domain with a rate of 0.1 - 0.3 ppb/h over most of the rainband. Enhanced rates were seen at the top of cloud, being about 0.5 ppb/h with a maximum rate of 0.9 ppb/h seen in the trailing edge. These rates agree well with theoretical rates calculated by Chameides and Davis (1982), McElroy (1986), and Walcek (1988) who all used more detailed gas-phase mechanisms.

Over the three hours of simulation time it was found that this additional H_2O_2 had a small effect on the sulphate produced. As expected, any increase in production was seen after 30 min. when the depletion of H_2O_2 became pronounced. In cloud, there was an increase of 10% in the amount of sulphate produced and in rain the increase was 23%. The bulk of the oxidation still occurred at and below cloud base. It was found that at these levels, oxidation was limited by the peroxide available for reaction but higher in the band, the reaction was limited by SO_2. Low in the rainband there was a net loss of H_2O_2 and higher in the band a net production was observed. In this study, the increased SO_4^{2-} production did not alter the amount of SO_4^{2-} deposited to the ground because of the large mass of sulphate that entered cloud by nucleation or scavenging of aerosol.

5.3 Limitations of parameterization method

In any modelling study, the usefulness of the results cannot be fully appreciated unless the areas of model uncertainty are noted. In this study, there are some uncertainties associated with the method chosen to estimate in-cloud H_2O_2 production. As stated in Chapter 3, a simple set of gas-phase reactions has been used to provide a first approximation to gas-phase production and concentrations of HO_2. Although the set is incomplete, the dominant reactions have been included and results agree well with other reported results. The simplicity of the scheme allowed it to be included in the complex rainband chemistry model which a more complex scheme would not have allowed.

Uncertainties lie in the concentrations of NO and CO used in the model. These were fixed at values for moderately polluted conditions but different concentrations of these species would affect the HO_2 to OH ratio. The dominant loss mechanism for HO_2 by gas-phase reactions is its reaction with NO. When scavenging is efficient, however, the loss to cloud dominates and competes with the NO reaction for HO_2. McElroy (1986) has suggested that under polluted conditions, because HO_2 scavenging by cloud was faster than loss of HO_2 with NO, H_2O_2 production in cloud is more important than the H_2O_2 production in air.

In this study, the oxidation of SO_2 by OH radicals in the aqueous phase has not been included. The scavenging of OH radicals from the gas phase is thought to be slow and it was not considered to be an important oxidant. The reaction of O_2^- and O_3 produces OH radicals and Pandis and Seinfeld (1989) have suggested that the oxidation of S(IV) by OH could be significant. This reaction perhaps deserves further study.

As discussed in Chapter 2, uncertainties exist also in the values reported from observations and the extrapolations made to create model initial chemical profiles. In the model, profiles of ammonia and nitric acid were assumed to follow the SO_2 profiles and gas-phase H_2O_2 was not measured in the rainband study at all. Observations showed that concentrations of SO_2 and sulphate varied considerably across the rainband and the variability must be taken into account when comparisons are made.

5.4 Suggestions for further research

There are several further experiments that could be performed with the model to test it. First of all, chemistry results under different polluted conditions could be examined. Also a more complete set of observations would allow a more thorough evaluation of model performance. Because the initial H_2O_2 concentrations play a large role in determining the amount of SO_4^{2-} produced, observations that included vertical profiles of H_2O_2 would be valuable.

The base-state diffusion scheme, as discussed in Chapter 4, tends to decrease the effects of vertical transport of chemicals in the cloud. The inclusion of a diffusion scheme that could still approximate the subsidence outside the band area but not overcompensate for the effects of advection in the band would be an improvement.

Finally, the parameterization method could be used in other models to investigate effects of H_2O_2 production in other cloud types.

REFERENCES

Barth, M.C., D.A. Hegg, P.V. Hobbs, J.G. Walega, G.L. Kok, B.G. Heikes, A.L. Lazrus, 1989: Measurements of atmospheric gas-phase and aqueous-phase hydrogen peroxide concentration in winter on the east coast of the United States. *Tellus*, **41B**, 61-69.

Brasseur, Guy, and Susan Solomon, 1984: *Aeronomy of the Middle Atmosphere*, D. Reidel Publishing Company, Dordrecht, Holland, 441 pp.

Calvert, Jack G., Allan Lazrus, Gregory L Kok, Brian G. Heikes, James G. Walega, John Lind and Christopher A. Cantrell, 1985: Chemical mechanisms of acid generation in the troposphere. *Nature*, **317**, 27-35.

Chameides, William L., 1984: The Photochemistry of a Remote Marine Stratiform Cloud. *J. Geophys. Res.*, **89**, 4739-4755.

--------, and D.D. Davis, 1982: The Free Radical Chemistry of Cloud Droplets And Its Impact Upon the Composition of Rain. *J. Geophys. Res.*, **87**, 4863-4877.

Chang, C.-C., 1984: A Case Study of Wet Deposition in Solution and Central Ontario. Master's Thesis, McGill University, 106 pp.

Cho, H.R. and J.V. Iribarne, 1983: *The Role of Clouds and Precipitation in Long-Range Transport and Acid Rain in Eastern Canada, Vol 1 & 2*, Report for the Canadian Electrical Assoc., Montreal, Quebec CEA No. 217 G348.

Daum, P. H., T.J. Kelly, S.E. Schwartz, and L. Newman, 1984: Measurements of the Chemical Composition of Stratiform

Clouds. *Atmos. Environ.* **18**, 2671-2684.

Demerjian, Kenneth L., Kenneth L. Schere, and James T. Peterson, 1980: Theoretical Estimates of Actinic (Spherically Integrated) Flux and Photolytic Rate Constants of Atmospheric Species in the Lower Troposphere. *Advances in Environmental Science and Technology* **10**, 369-459.

Dickerson, R.R., D.H. Stedman, W.L. Chameides, P.J. Crutzen, and J. Fishman, 1979: Actinometric Measurements and Theoretical Calculations of $j(O_3)$, The Rate of Photolysis of Ozone to $O(^1D)$. *Geophys. Res. Lett.*,**6**, 833-836.

Fiocco, G., A. Mugnai, W. Forlizzi, 1978: Effects of Radiation Scattered by Aerosols on the Photodissociation of Ozone. *J. of Atmos. and Terr. Physics*, **40**, *949-961.*

Flossmann, A.I., W.D. Hall, H.R. Pruppacher, 1985: A Theoretical Study of the Wet Removal of Atmospheric Pollutants. Part I: The redistribution of Aerosol Particles Captured through Nucleation and Impaction Scavenging by Growing Cloud Drops. *J. Atmos. Sci.*, **42**, 582-606.

Flossmann, A.I., H.R. Pruppacher, J.H. Topalian, 1987: A Theoretical Study of the Wet Removal of Atmospheric Pollutants. Part II: The Uptake and Redistribution of $(NH_4)_2SO_4$ Particles and SO_2 Gas Simultaneously Scavenged by Growing Cloud Drops. *J. Atmos. Sci.*, **44**, 2912-2923.

Giles, Andrew, 1987: The influence of the ice phase on the simulated chemistry of a rainband. MSc thesis, Dept. of Meteorology, McGill University. 118 pp.

Hales, Jeremy, 1982: Mechanistic analysis of precipitation scavenging using a one-dimensional, time-variant model. *Atmos. Environ.*, **16**, 1775-1783.

Hegg, D.A., S.A. Rutledge, and P.V. Hobbs, 1984: A Numerical Study for Sulfur Chemistry in Warm-Frontal Rainbands. *J. Geophys. Res.*, **89**, 7133-7147.

----, ----, ----, 1986: A Numerical Model For Sulfur and Nitrogen Scavenging in Narrow Cold-Frontal Rainbands 2. Discussion of Chemical Fields. *J. Geophys. Res.*, **91**, 14,403-14,416.

Heikes, Brian G., Gregory L. Kok, James G. Walega, and Allan L. Lazrus, 1987: H_2O_2, O_3 and SO_2 Measurements in the Lower Troposphere Over the Eastern United States During Fall. *J. Geophys. Res.*, **92**, 915-931.

Hoffmann, Michael R., 1986: On the Kinetics and Mechanism of Oxidation of Aquated Sulfur Dioxide By Ozone. *Atmos. Environ.*, **20**, 1145-1154.

Hong, M.S., G.R. Carmichael, 1983: An investigation of sulphate production in clouds using a flow-through chemical reactor approach. *J. Geophys. Res.*, **88**, 10,733-10,744.

Hough, A., 1987: A computer modelling study of the chemistry occurring during cloud formation over hills. *Atmos. Environ.*, **21**, 1073-1095.

Isaac, G.A., W.R. Leaitch, J.W. Strapp, K.G. Anlauf, J.W. Bottenheim, H.A. Wiebe, and K.J. Puckett, 1988: Canadian airborne cloud measuremants for model evaluation Preliminary results from the 1988 Muskoka field study.

Preprints, Symposium on the role of Clouds in Atmospheric Chemistry and Global Climate, American Meteorology Society, 225-230.

Isaac, G.A., and J.W. Strapp, H.A. Wiebe, W.R. Leaitch, J.B. Kerr, K.G. Anlauf, P.W. Summers, J.I. MacPherson, 1983: The Role of Cloud Dynamics in Redistributing Pollutants and the Implications for Scavenging Studies. *Precipitation Scavenging, Dry Deposition and Resuspension.* H.R. Pruppacher, R.G. Semonin and W.G.N. Slinn, coords., Elsevier, New York, pp 1-13.

Jacob, D.J. and M.R. Hoffmann, 1983: A dynamic model for the production of H^+, NO_3^-, and SO_4^{2-} in urban fog. *J. Geophys. Res.*, **88**, 6611-6621.

Joseph, J.H., W.J. Wiscombe, and J.A. Weinman, 1976: The delta-Eddington approximation for radiative flux transfer. *J. Atmos. Sci.*, **33**, 2452-2459.

Kok, Gregory L., 1980: Measurements of H_2O_2 in rainwater. *Atmos. Environ.*, **14**, 653-656.

Kelly, Thomas J., Peter H. Daum, and Stephen E. Schwartz, 1985: Measurements of Peroxides in Cloudwater and Rain. *J. Geophys. Res.*1.

Kreitzberg, Carl W., 1984: Models of the Effects on Acid Precipitation of Air Motions in Different-Size Storms, in *Meteorological Aspects of Acid Rain*, edited by Chandrakant M. Bhumralkar, pp. 103-118, Butterworth Publishers, Stoneham, MA.

Lee, I-Y., 1986: Numerical simulation of chemical and physical properties of cumulus clouds. *Atmos. Environ.*, **20**, 767-771.

Leighton, H.G., 1980: Application of the delta-Eddington Method to the Absorption of Solar Radiation in the Atmosphere. *Atmos. Ocean*, **18**, 43-52.

Maahs, H.G., 1983: Kinetics and mechanisms of the oxidation of S(IV) by ozone in aqueous solution with particular reference to SO_2 conversion in nonurban tropospheric clouds. *J Geophys. Res.*, **88**, 10,721-10,732.

Madronich, Sasha, 1987: Photodissociation in the Atmosphere 1. Actinic Flux and the Effects of Ground Reflections and Clouds. *J. Geophys. Res.*, **92**, 9740-9752.

Martin, L.R., 1983: Kinetic studies of sulfite oxidation in aqueous solution. In *SO2, NO, and NO2 oxidation mechanisms: atmospheric considerations*. J.G. Calvert, Ed., Butterworth, 254 pp.

McElroy W.J., 1986: Sources of Hydrogen Peroxide in Cloudwater. *Atmos. Environ.*, **20**, 427-438.

Mozurkewich, Michael, Peter H. McMurry, Anand Gupta, and Jack G. Calvert, 1987: Mass Accommodation Coefficient for HO_2 Radicals on Aqueous Particles. *J. Geophys. Res.*, **92**, 4163-4170.

Niewiadomski, M., 1989: Sulphur dioxide and sulphate in a three-dimensional field of convective clouds: numerical simulations. *Atmos. Environ.*, **23**, 477-487.

-------, 1986: A passive pollutant in a three-dimensional field of convective clouds: Numerical simulations. *Atmos. Environ.*, **20**, 139-145.

Pandis, Spyros N., and John H. Seinfeld, 1989: Sensitivity

Analysis of a Chemical Mechanism for Aqueous-Phase Atmospheric Chemistry. *J. Geophys. Res.*, **94**, 1105-1126.

Penndorf, R., 1957: Tables of the refractive index for standard air and the Rayleigh scattering coefficient for the spectral region between 0.2 and 20.0 μm and their application to atmospheric optics. *J. Opt. Soc. Am.*, **47**, 176-182.

Pitre, J.S., 1986: The Role of Oxidation in the Chemistry of a Rainband. MSc thesis, Dept. of Meteorology, McGill University. 115 pp.

Rutledge, S.A., D.A. Hegg, and P.V. Hobbs, 1986: A Numerical Model for Sulfur and Nitrogen Scavenging in Narrow Cold frontal Rainbands 1. Model Description and Discussion of Microphysical Fields. *J. Geophys. Res.*, **91**, 14,385-14,402.

Rutledge, S.A. and P.V. Hobbs, 1983: The mesoscale and microscale scale structure and organization of clouds and precipitation in midlatitude cyclones. VIII: A model for the "seeder-feeder" process in warm-frontal rainbands. *J. Atm. Sci.*, **40**, 1185-1206.

Schwartz, Stephen E., 1984a: Both Sides Now: The Chemistry of Clouds. New York Academy of Sciences.

-------, 1984b: Gas- and Aqueous-Phase Chemistry of HO_2 in Liquid Water Clouds. *J. Geophys. Res.*, **89**, 11,589-11,598.

-------, 1986: Mass-transport considerations pertinant to aqueous-phase reactions of gases in liquid water clouds. *Chemistry of Multiphase Atmospheric Systems*. W. Jaeschke, ed., NATO ASI Series Vol G6, Springer-

Verlag, Berlin.

Scott, B.C., 1978: Parameterization of Sulfate Removal by Precipitation. *J. Appl. Met.*, **17**, 1375-1389.

Seigneur, Christian, and Praedeep Saxena, 1988: A Theoretical Investigation of Sulfate Formation in Clouds. *Atmos. Environ.*, **22**, 101-115.

-----,and -----, 1984: A Study of Atmospheric Acid Formation in Different Environments. *Atmos. Environ.*, **18**, 2109-2124.

Seinfeld, John H., 1986: *Atmospheric Chemistry and Physics of Air Pollution*, Wiley, New York, 738 pp.

Stephens, G.L., 1979: Optical Properties of Eight Water Cloud Types, Commonwealth Scientific and Industriel Research Organization, Division of Atmospheric Physics, Technical Paper No. 36, Australia.

Tremblay, A., 1987: Cumulus cloud transport, scavenging and chemistry: Observations and simulations. *Atmos. Environ.*, **21**, 2345,2364.

------- and H.G. Leighton, 1984: The influence of cloud dynamics upon the redistribution and transformation of SO_2-A numerical simulation. *Atmos. Environ.*, **9**, 1885-1894.

-------,and -------, 1986: A three-dimensional cloud chemistry model. *J. Climate Appl. Meteor.*, **25**, 652-671.

Walcek, Chris J., 1988: The Influence of Radiative and Dynamic Cloud Structure on the Formation of H_2O_2 in Cloud Updrafts. Preprints, Symposium on the Role of

Clouds in Atmospheric Chemistry and Global Climate, American Meteorological Society, J15-17.

------ and G.R. Taylor, 1986: A theoretical method for computing vertical distributions of acidity and sulfate production within cumulus clouds. *J. Atmos. Sci.*, **43**, 339-355.

Wiscombe, W.J., 1977: The delta-Eddington approximation for a vertically inhomogeneous atmosphere. Tech. Note NCAR/TN-121, National Center for Atmospheric Research, Boulder, Colo.

Valton, A.M., 1986: Cloud Dynamic-Pollutant Interactions in a Rainband. MSc thesis, Dept. of Meteorology, McGill University. 124 pp.

Zika R., E. Saltzman, W.L. Chameides, and D.D. Davis, 1982: H_2O_2 Levels in Rainwater Collected in South Florida and the Bahama Islands, *J. Geophys. Res.*, **87**, 5015-5017.